Available online at www.sciencedirect.com
SCIENCE DIRECT®
Lithos 66 (2003) 241–273
LITHOS
www.elsevier.com/locate/lithos

Highly fractionated I-type granites in NE China (I): geochronology and petrogenesis

Fu-yuan Wu[a,b], Bor-ming Jahn[b,*], Simon A. Wilde[c], Ching-Hua Lo[d], Tzen-Fu Yui[e], Qiang Lin[a], Wen-chun Ge[a], De-you Sun[a]

[a] *Department of Geology, Jilin University, 79 Jianshejie, 130061 Changchun, China*
[b] *Géosciences Rennes (CNRS), Université de Rennes I, Avenue du Général Leclerc, F-35042 Rennes cedex, France*
[c] *School of Applied Geology, Curtin University of Technology, Perth, Western Australia, 6845, Australia*
[d] *Department of Geology, National Taiwan University, 245 Choushan Road, Taipei, 10770, Taiwan*
[e] *Institute of Earth Sciences, Academia Sinica, P.O. Box 1-55, Nankang, Taipei 11529, Taiwan*

Received 25 January 2001; accepted 18 September 2002

Abstract

Northeastern (NE) China is the easternmost part of the Central Asian Orogenic Belt (CAOB), which is celebrated for its accretionary tectonics and the world's most important juvenile crust production in the Phanerozoic era. Abundant granitoids occur in the Great Xing'an, Lesser Xing'an and Zhangguangcai Ranges in NE China. This paper presents partial results of a series of studies on the granitoids from this region, aiming to understand their role in the building of new continental crust in eastern Asia. Three composite granite plutons (Xinhuatun, Lamashan and Yiershi) were chosen for geochemical and isotopic study in order to determine their emplacement ages and petrogenesis. Petrographically, they range from granodiorite (minor), monzogranite, syenogranite to alkali-feldspar granite. Quartz and perthitic feldspar are principal phases, accompanied by minor amounts of plagioclase, biotite (< 5%) and other accessory minerals. In addition, many contain abundant miarolitic cavities which suggest that they were emplaced at shallow levels with extensive fractional crystallization. Geochemically, the granites are silica-rich, peraluminous and have high contents of alkalis. They invariably show enrichment in light rare earth elements (LREE) and significant negative Eu anomalies. All the granitic rocks demonstrate the characteristic negative anomalies in Ba, Nb, Sr, P, Eu, and Ti, and a positive anomaly in Pb in the spidergram.

The emplacement of the Xinhuatun pluton took place at 184 ± 4 Ma as revealed by zircon SHRIMP U–Pb data. This is also supported by the slightly younger Rb–Sr whole-rock (WR) isochron age of 173 ± 3 Ma. A whole-rock (WR) Rb–Sr isochron age of 154 ± 3 Ma was obtained for the Lamashan pluton, which is interpreted as close to the time of emplacement. The Yiershi pluton was intruded at about 140 Ma as evidenced by a zircon U–Pb age of 137 ± 2 Ma and WR Rb–Sr isochron age of 143 ± 5 Ma. Biotite-WR Rb–Sr isochrons and $^{40}Ar/^{39}Ar$ ages of feldspars allow us to estimate the cooling rate of each pluton.

Geochemical data suggest that the rocks are highly fractionated I-type granites. Fractionation of biotite and feldspars was the principal process of magmatic differentiation and responsible for major element variation. Rb, Sr and Ba concentrations

* Corresponding author. Tel.: +33-2-23-23-60-83; fax: +33-2-23-23-56-80.
E-mail address: jahn@univ-rennes1.fr (B. Jahn).

0024-4937/02/$ - see front matter
PII: S0024-4937(02)00222-0

were controlled by feldspar separation, whereas REE elements were fractionated by accessory minerals, such as apatite, allanite and monazite.

Keywords: NE China; Central Asian Orogenic Belt; Granite; I-type granite; Geochronology; Geochemistry

1. Introduction

Northeastern (NE) China is characterized by widespread Phanerozoic granitic rocks, which are traditionally regarded as of late Paleozoic (“Hercynian”) age. According to regional geological surveys, the granites comprise at least 50% of the area in the mountainous regions (JBGMR, 1988;

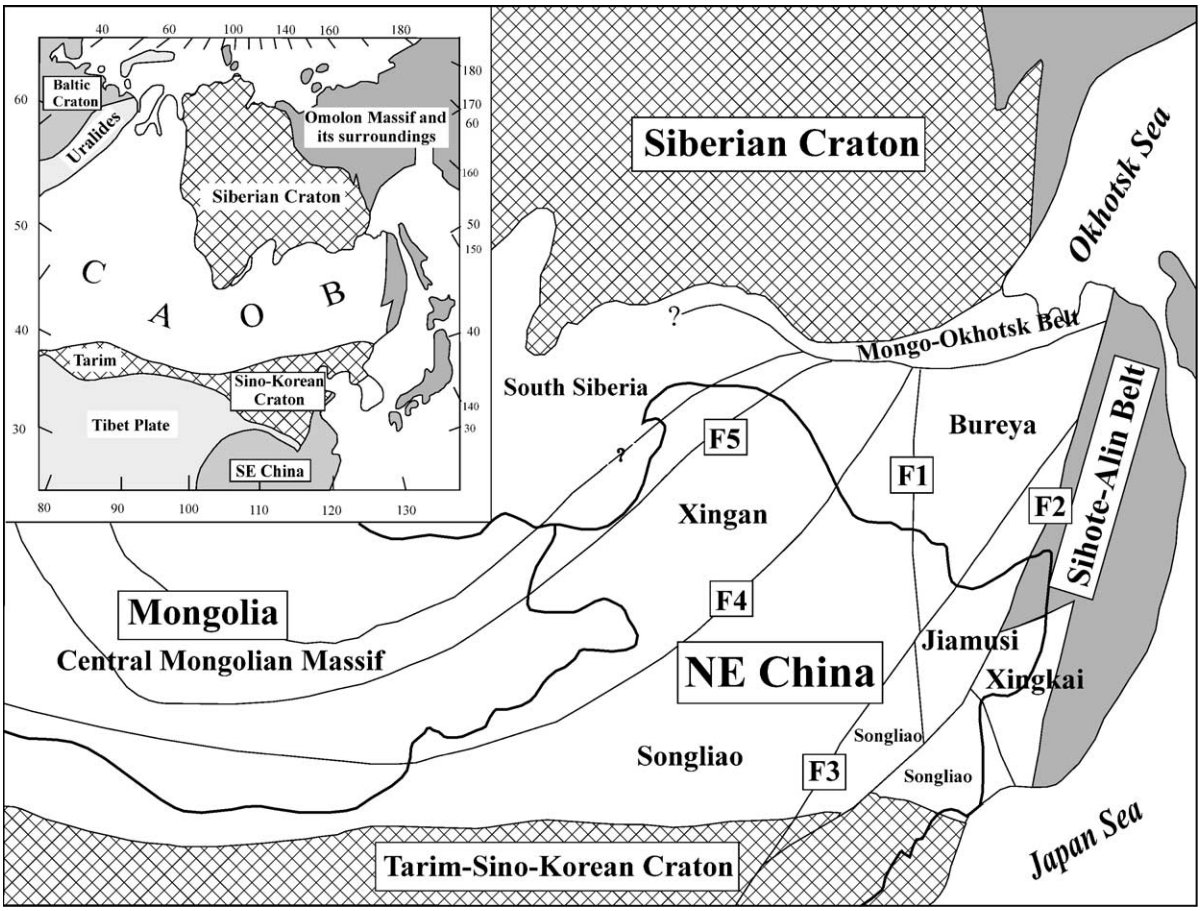

Fig. 1. Tectonic map of the Xingmeng (Xing’an–Mongolian) Orogenic Belt in the eastern part of the CAOB (Central Asian Orogenic Belt). The belt consists of several microcontinental blocks including the Jiamusi block and its northern extension in Bureya (Russia), the Songliao and Xing’an blocks, etc. All these blocks contain small proportions of Precambrian basement rocks. Major faults—F1: Mudanjiang fault, F2: Dunhua–Mishan Fault (northern branch of the Tanlu Fault), F3: Yitong–Jiamusi Fault, F4: Nenjiang–Hegenshan Fault, F5: Derbugan–Southern Mongolia Fault.

HBGMR, 1993; IMBGMR, 1990), such as the Zhangguangcai Range in the east, Great Xing'an Range in the west and Lesser Xing'an Range in the north (Wu et al., 2000). Furthermore, underneath the flat-lying Songliao Basin, much of the basement is also composed of granites (Wu et al., 2001). Thus, NE China may be considered as a super-giant granitic province.

A few isotopic age data suggest several periods of granitic intrusions from early Paleozoic to Mesozoic (JBGMR, 1988; IMBGMR, 1990; HBGMR, 1993; Qin et al., 1998, 1999), but these results are published in Chinese journals or books, and thus not easily accessible. Moreover, our recent field and geochronological investigations indicate that the Paleozoic granites are only present in the Jiamusi Block in the east and in the Great Xing'an Range in the west (Wu et al., 2000, 2001, 2002); most other granites are of Mesozoic age.

The extensively exposed Mesozoic I- and A-type granitoids in NE China (almost 100,000 km^2) are little known in the western literature. Several hundreds of plutons occur throughout the Xing'an and Songliao blocks (Fig. 1). Petrographically, they range from granodiorite (minor), monzogranite, syenogranite to alkali-feldspar granite and alkaline granite. Quartz and perthitic feldspar are the principal phases, accompanied by minor amounts of plagioclase, ferromagnesian and other accessory minerals. Mafic alkaline minerals, such as arfvedsonite and aegirine-augite, are found only in the alkaline granites. In addition, many contain abundant miarolitic cavities which suggest that they were generally emplaced at shallow levels with extensive fractional crystallization. Most granites contain biotite (<5%) as the only mafic mineral. Mafic enclaves are rare. The generation of this kind of fractionated granite has rarely been studied (Champion and Chappell, 1992).

Though the Phanerozoic granites are widespread in NE China, few of them have been precisely dated. The absence of good age data hampers our understanding of the time–space relationship of the massive distribution of granitic rocks in NE China. In this paper, we present new U–Pb, Rb–Sr and Ar isotopic age data for three plutons of felsic I-type granites to determine their emplacement histories and cooling rates. In the companion paper (part II), Sr–Nd–O isotopic and trace element data will be presented to constrain their petrogenesis; some important implications for the continental crustal growth in the Phanerozoic will be discussed.

2. Geological setting

The study area is traditionally considered as the eastern segment of the Xingmeng Orogenic Belt (Xingmeng = Xing'an and Mongolia or Khingan–Mongolian), which constitutes the eastern part of the Central Asian Orogenic Belt (CAOB, Fig. 1). NE China represents a collage of three microcontinental blocks (Ye et al., 1994; Wu et al., 1995): the Jiamusi Block in the east, Songliao Block in the centre and Xing'an Block in the northwest (Fig. 1). The three blocks are separated by the Mudanjiang (F1) and Nenjiang (F4) faults. Distinct geological characteristics and geophysical properties separate the individual blocks (Ye et al., 1994).

The Jiamusi Block is characterized by two sequences of Precambrian metamorphic rocks—the Mashan and Heilongjiang Groups. The Mashan Group comprises granulite, marble, graphitic schist (of khondalitic affinity), together with gneiss and garnet-bearing granite. It was metamorphosed to the granulite facies 500 Ma ago (Wilde et al., 1997, 2000). The Heilongjiang Group, exposed along the Mudanjiang Fault between the Jiamusi and Songliao Blocks, is characterized by highly deformed blueschist facies rocks including glaucophane schist, marble and chert.

The Songliao Block is mostly restricted by the Songliao sedimentary basin. Its eastern and northern parts are the Zhangguangcai and Lesser Xing'an Ranges which are characterised by voluminous Phanerozoic granitic rocks. Proterozoic metamorphic rocks with banded iron formations (Dongfengshan Group) occur in the eastern Lesser Xing'an and northern Zhangguangcai Ranges, where a change from a passive continental margin in the Cambrian to an active margin in the Silurian has been identified (HBGMR, 1993). Recent borehole data from the Songliao Basin reveal that granites are widespread and form the basement of the basin (Wu et al., 2001).

The Xing'an Block, located in the Great Xing'an Range, is characterized by extensive Mesozoic vol-

canic and granitic rocks. Proterozoic metamorphic rocks also occur in the northern part, and Paleozoic strata are well developed, especially in the southern part.

A tectonic affinity between the Xing'an block and the Siberia continent or the Central Mongolian Massif has been suggested based on paleomagnetic data (Zonenshain et al., 1990). However, the origin of the Songliao and Jiamusi blocks remains controversial (Tang et al., 1995). According to Zonenshain et al. (1990), these two blocks constitute part of the Khingan–Bureya Massif, which is distinguished in its tectonic evolution from Siberia and other adjacent cratons.

The assemblage of the Jiamusi and Songliao blocks probably took place in the Silurian based on several lines of evidence: (1) identification of an Ordovician arc assemblage on the eastern margin of the Songliao block; (2) occurrence of blueschists with metamorphic ages of ca. 600–560 Ma (Zhang, 1992); (3) an ophiolitic melange in which middle Ordovician–Silurian radiolaria-bearing siliceous rocks occur along the Mudanjiang Fault; (4) intrusion of calc-alkaline granites at 435–400 Ma (HBGMR, 1993); and (5) deposition of Devonian shallow-water sedimentary rocks. The Jiamusi–Songliao composite block was then accreted to the Xing'an block along the Nenjiang fault during the late Devonian to early Carboniferous (Ye et al., 1994; Yu et al., 1996), followed by development of a regional extensional system (Tang, 1990; Wu et al., 1995).

A major controversy concerns the timing of collision between the North China Block (NCB) and the composite Xingmeng Block (now the eastern part of the Central Mongolian microcontinent). It has been suggested that collision took place in the late Triassic (Zonenshain et al., 1985, 1990), but recent paleomagnetic data suggest that the Xingmeng and the NCB were amalgamated before the late Permian, and then collided with the Siberian plate when the Mongolia–Okhotsk Ocean was closed in the late Jurassic (Zhao et al., 1990).

In the Xingmeng belt, available age data indicate three distinct periods of granite magmatism: (1) late Paleozoic (300–250 Ma), with emplacement of calc-alkaline rocks (diorite, tonalite and granodiorite) and late A-type granites (Hong et al., 1994; HBGMR, 1993; Wu et al., 2000, 2001, 2002; Sun et al., 2001); (2) Triassic to Jurassic, with highly fractionated I- and A-type granitoids (in Wu et al., 2002 and to be discussed below); and (3) Cretaceous, with I-type granites (granodiorite, monzogranite and syenite), followed by A-type granites (Li and Yu, 1993; Wang and Zhao, 1997; Jahn et al., 2001; Wu et al., 2002). The Mesozoic A-type granites are typically anorogenic, and are genetically related to extension in eastern China during the Yanshan Orogeny (Jurassic–Cretaceous, HBGMR, 1993).

3. Sample description

Representative rock types were selected from three plutons (Xinhuatun, Lamashan and Yiershi) for geochemical and isotopic studies (Fig. 2). These plutons were previously considered to be the most typical Triassic granites in NE China (HBGMR, 1993), and there is a need to verify their emplacement ages and to study their petrology and petrogenesis. The samples were taken from the freshest outcrops available at each locality. However, most samples still show effects of weathering and, in some instances, hydrothermal alteration as indicated by sericitization of feldspar and partial chloritization of biotite. Lithologic classification of the analyzed granites is based on the visually estimated modes in hand specimens and in thin sections (Table 1), as well as from chemical analyses (Table 2).

3.1. Xinhuatun (samples prefixed with X-)

The Xinhuatun pluton is located about 60 km to the east of Harbin, capital of Heilongjiang Province (Fig. 2a), and has an outcrop area of ca. 160 km^2 (Fig. 2b). It is intruded into Upper Paleozoic–Lower Mesozoic strata, and covered by late Mesozoic volcanic and clastic sedimentary rocks. The rock types range from granodiorite, monzogranite to syenogranite, and they consist mainly of quartz, perthite and plagioclase with minor amount of biotite. In some cases, banding of the rock results from distinct biotite layers. Biotite-bearing rock corresponds to granodiorite which contains plagioclase phenocrysts and shows a hypidiomorphic-granular texture. The accessory mineral assemblage is magnetite, apatite, zircon, monazite and titanite. With a decreasing

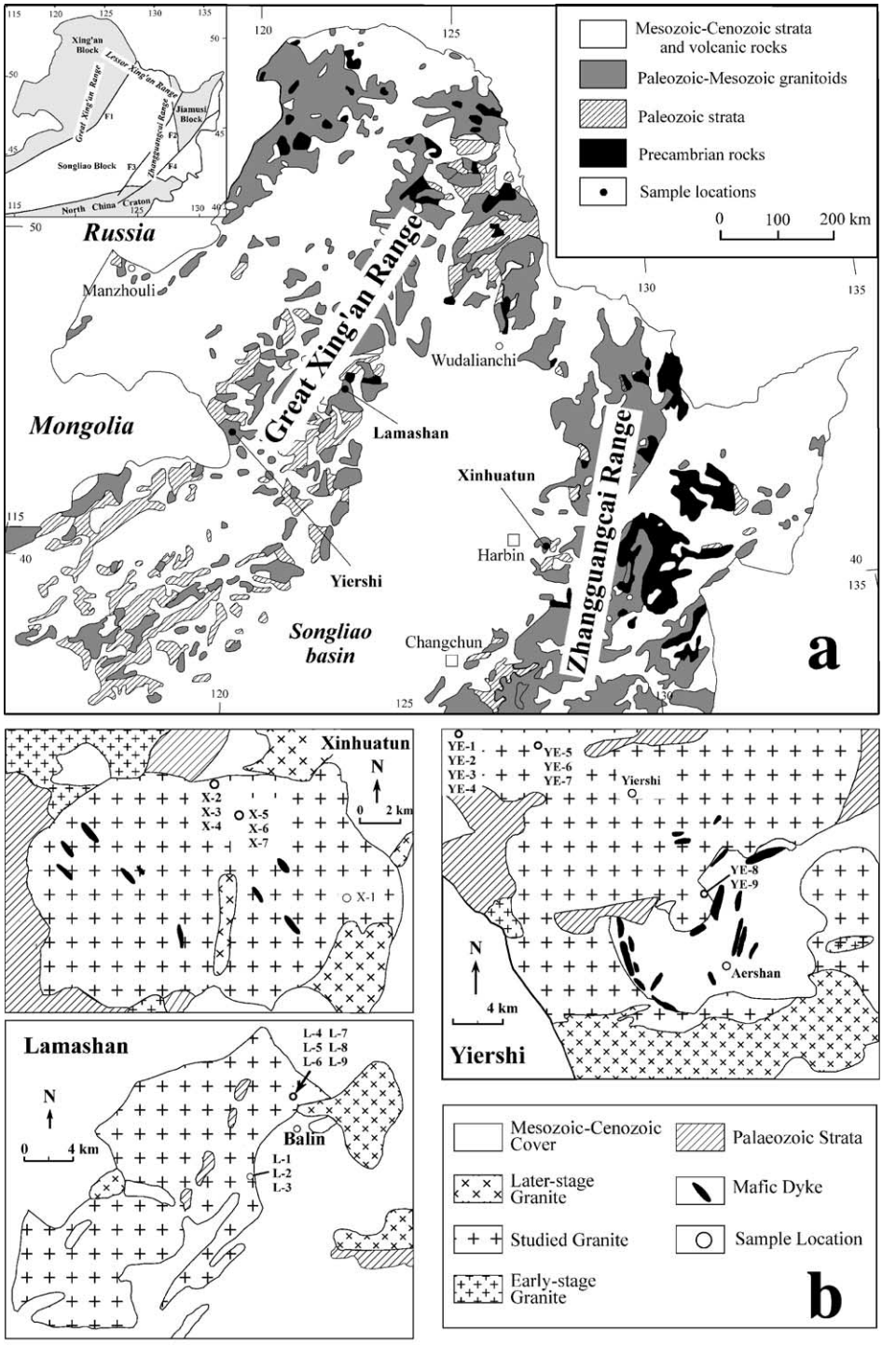

Fig. 2. Simplified geological map of NE China showing the sampling localities in the Xinhuatun, Lamashan and Yiershi granitic plutons. Xinhuatun is situated in the Zhangguangcai Range in the east, whereas the other two plutons are in the Great Xing'an (Khingan) Range in the west. The Songliao Basin separates both ranges.

Table 1
The description of studied granitic samples in NE China

Pluton	Sample No.	Rock type	Texture	Bi	Q (%)	Kf (%)	Pl (%)	Note
Xinhuatun	X-1	Syenogranite	Coarse	Trace (altered)	20	70	10	Zoned Pl
	X-2	Adamellite	Medium	5%	25	30	40	Banded Bi
	X-3	Granodiorite	Coarse	10%	20	10	60	Banded Bi
		Kf granite	Fine		30	70		
	X-4	Granodiorite	Medium	10%	20	10	60	Banded Bi
	X-5	Diorite enclave	Medium	10%	10		80	
	X-6	Syenogranite	Medium	5%	30	50	15	
	X-7	Kf granite	Medium	2%	35	58	5	
Lamashan	L-1	Adamellite	Coarse	Trace	30	35	35	Miarolitic
	L-2	Adamellite	Coarse	Trace	30	40	30	Miarolitic
	L-3	Adamellite	Coarse	Trace	20	40	40	Miarolitic
	L-4	Syenogranite	Coarse	Trace	40	50	10	Miarolitic
	L-5	Kf granite	Coarse	Trace	30	65	5	Miarolitic
	L-6	Syenogranite	Coarse	Trace	30	60	10	Miarolitic
	L-7	Syenogranite	Coarse	Trace	40	50	10	Miarolitic
	L-8	Syenogranite	Coarse	Trace	40	50	10	Miarolitic
	L-9	Kf granite	Fine	Trace	50	45	5	Miarolitic
Yiershi	YE-1	Kf granite	Coarse	Trace (altered)	30	70		Granophyric
	YE-2	Kf granite	Fine	Trace (altered)	30	70		Granophyric
	YE-3	Syenogranite	Coarse	Trace	30	60	10	
	YE-4	Kf granite	Medium	Trace	30	70		Granophyric
	YE-5	Syenogranite	Coarse	5%	30	50	15	
	YE-6	Kf granite	Fine	Trace (altered)	30	65	5	Aplitic
	YE-7	Kf granite	Fine	Trace (altered)	30	65	5	Aplitic
	YE-8	Kf granite	Medium	Trace (altered)	30	70		
	YE-9	Syenogranite	Coarse	5%	35	50	10	

amount of biotite, the rock changes from granodiorite, to monzogranite, syenogranite and finally to granophyre. This suggests that this pluton has undergone significant fractional crystallization. Hexagonal quartz is present in monzogranite and syenogranite, and small microgranular enclaves containing acicular crystals of apatite are also present.

3.2. Lamashan (prefixed with L-)

The Lamashan pluton, located in the Great Xing'an Range, crops out over 25 km^2 (Fig. 2). It is intruded into older granites (Paleozoic?) and covered by Jurassic volcanic rocks. It has been considered as a typical pluton emplaced during the late Paleozoic (HLBMR, unpublished), but no precise age data are available. The pluton is made up mainly of medium- to coarse-grained granitoids, including monzogranite, syenogranite and alkali-feldspar granite. Locally, they are cut by centimetre- to decimetre-wide veins of fine-grained, grey alkali-feldspar granite and granophyre. Most of the granitic rocks show miarolitic cavities, and the late-stage granophyre displays a graphic texture. The major mineral phases are perthite, quartz and plagioclase. The Lamashan granites are distinguished from the Xinhuatun pluton by the small amount of biotite and presence of hexagonal quartz in all the rock types. Mafic enclaves are rare. The graphic texture and hexagonal quartz are indicative of shallow emplacement.

3.3. Yiershi (prefixed with YE-)

The Yiershi pluton (≈ 400 km^2) occurs near the border of China and Mongolia (Fig. 2). It is intruded into Paleozoic sediments and cut by late-stage dikes and covered by Late Mesozoic volcanic rocks. The rock types range from medium- to coarse-grained syenogranite, alkali-feldspar granite and miarolitic granite in the early stage, to fine-grained granite in the late stage. The granite is made up principally of

quartz and perthite, with plagioclase less than 15%. In contrast, in the late-stage fine-grained granite, the alkali-feldspar often displays a thin albitic rim. Primary biotite is generally lacking, except in earlier intrusive phases, quartz is hexagonal in most cases, but feldspars (mostly alkali-feldspar) are subhedral to anhedral. In some cases, intergrowth of quartz and feldspar forms the graphic texture. The main accessory phases are apatite, magnetite, allanite and zircon.

4. Analytical techniques

4.1. Major and trace elements

Major and trace element (except rare earth elements) abundances were determined by X-ray fluorescence spectrometry (XRF) using a Philips PW1480 spectrometer at the Université de Rennes 1. Analytical uncertainties range from 1% to 3% for major elements; 5% for trace elements with concentrations >20 ppm and 10% for those <20 ppm. REE abundances were determined by the isotope dilution method using the routine procedures employed at Rennes (Jahn et al., 1996). Overall analytical uncertainties are 3% for all rare earth elements. In order to demonstrate the reliability of the analytical results, six samples (two from each pluton) were further analyzed using the ICP-MS method in Nancy, France, which employed a method of sample dissolution including fusion of rock powder with lithium borate ($LiBO_2$) flux. The results of isotopic dilution and ICP-MS are in good agreement (Table 2), particularly for REE abundances.

4.2. Zircon U–Pb analyses

Zircon crystals were extracted by crushing and use of a combination of heavy liquid and magnetic separation techniques. Individual crystals were handpicked and mounted, along with several pieces of the Curtin University standard (CZ3—which has a conventionally measured $^{206}Pb/^{238}U$ age of 564 Ma (Pidgeon et al., 1994)), onto double-sided adhesive tape and enclosed in epoxy resin discs. The discs were polished, so as to effectively section the zircons in half, and then gold-coated.

U–Th–Pb analyses of the zircons were performed using the SHRIMP ion microprobe at Curtin University, following standard procedures described by Williams (1998) and Nelson (1999). Spot size ranged between 20 and 30 μm and each analysis spot was rastered over 120 μm for 5 min to remove any common Pb on the surface or contamination from the gold coating. The mass resolution used to measure Pb/Pb and Pb/U isotopic ratios ranged from 4770 to 5000 during three analytical session, and the Pb/U ratios were normalised to those measured on the standard zircon [CZ3—($^{206}Pb/^{238}U = 0.0914$)]. The error associated with the measurement of Pb/U isotopic ratios for the standard, at 1 standard deviation, was ~2% during each analytical run. The measured ^{204}Pb values in the unknowns were similar to those recorded for the standard zircon and so common lead corrections were made assuming an isotopic composition of Broken Hill lead, since the common lead is considered to be mainly associated with surface contamination in the gold coating (Nelson, 1999). The $^{206}Pb/^{238}U$ ages are considered to be the most reliable for concordant Phanerozoic zircons (Compston et al., 1992) because the low count rates on ^{207}Pb result in large statistical uncertainties, making the $^{207}Pb/^{206}Pb$ and $^{207}Pb/^{235}U$ ratios a less sensitive measure of age. Data reduction was performed using both the WAlead (Australian National University) and Krill 007 (P. D. Kinny, Curtin University) programs, applying the ^{208}Pb correction, since there is little evidence of post-crystallization disturbance to the U–Pb–Th systems of the younger zircons. Errors on individual analyses are based on counting statistics and are at the 1σ level. Errors on pooled analyses are quoted at 2σ or 95% confidence.

4.3. Sr isotopic analyses

Sr isotopic data were obtained using the method described by Jahn et al. (1996). Sample dissolution was carried out in sealed Savillex beakers for at least 7 days until no visible residues were observed. The same procedure was repeated when residue was observed after the first dissolution. The absence or insignificant amount of REE-carrying refractory minerals, such as zircon or monazite in the residue after dissolution, is clearly demonstrated in Table 2. Mass analyses were performed using a 7-collector Finnigan

Table 2
The chemical compositions of the highly fractionated granites from NE China

Analysis No.	12970	12971			12972	12973			12974	12975	12976
Sample No.	X-1	X-2			X-3	X-4			X-5	X-6	X-7
Major elements (wt.%, by XRF)											
SiO_2	76.41	73.88			76.54	68.91			63.00	76.51	75.47
Al_2O_3	12.70	12.55			12.45	13.45			17.37	12.39	12.92
FeO*	0.62	2.19			0.87	4.43			3.89	0.74	0.69
MnO	0.01	0.13			0.05	0.28			0.05	0.02	0.02
MgO	0.08	0.61			0.11	1.22			1.30	0.16	0.11
CaO	0.43	0.51			0.44	1.10			2.54	0.49	0.45
Na_2O	3.70	3.12			3.88	3.93			5.67	3.74	3.49
K_2O	4.61	5.16			4.27	3.88			1.58	4.45	4.82
TiO_2	0.08	0.31			0.13	0.62			0.57	0.11	0.11
P_2O_5	0.01	0.08			0.04	0.19			0.27	0.03	0.02
LOI	0.47	0.46			0.40	0.64			2.03	0.43	0.49
Total	99.1	99.0			99.2	98.7			98.3	99.1	98.6
Al/(Ca+Na+K)	1.07	1.08			1.05	1.06			1.11	1.04	1.10
Al/(Na+K)	1.15	1.17			1.13	1.26			1.57	1.13	1.18
Q	36.73	34.72			37.09	27.35			17.75	37.03	36.34
Or	27.61	30.94			25.54	23.39			9.70	26.66	29.03
Ab	31.74	26.79			33.24	33.93			49.85	32.08	30.10
An	2.10	2.04			1.95	4.30			11.25	2.27	2.14
Mg-Hy	0.20	1.54			0.28	3.10			3.36	0.40	0.28
Fe-Hy						1.69			0.61		
Ap	0.02	0.19			0.09	0.45			0.65	0.07	0.05
Ilm	0.02	0.60			0.11	1.20			1.12	0.04	0.04
Ru	0.07				0.07					0.09	0.09
Cor	0.88	1.11			0.75	1.27			2.45	0.61	1.21
Hem	1.67	1.47			1.71					1.69	1.69
Mag		0.57				3.08			3.03		
DI	98.18	94.49			97.82	88.97			88.55	98.04	97.61
Trace elements (in ppm, by XRF)			(ICP-MS)	Diff (%)			(ICP-MS)	Diff (%)			
Nb	11.5	16.9	14.70	−15	13.8	24.4	21.47	−14	12.4	20.8	19.2
Zr	79	150	135.07	−11	59	289	323.66	11	210	84	98
Y	4	12	12.09	1	7	24	21.67	−11	21	14	20
Sr	35	78	74.44	−5	31	121	115.52	−5	413	33	28
Rb	119	143	153.44	7	140	167	175.65	5	125	142	154
Co	<1	2	2.21	10	1	5	4.56	−10	8	<1	1
V	4	17	12.41	−37	7	36	28.56	−26	67	8	7
Ni	4	1	2.61	62	2	4	3.33	−20	3	2	2
Cr	9	3	0.28	−953	6	7	2.69	−160	5	3	4
Ba	416	1258	1109.56	−13	294	939	871.25	−8	501	174	131
Ga	15	15	16.23	8	13	19	20.75	8	21	14	14
Cu	3	2	2.39	16	<1	2	3.37	41	201	1	5
Zn	10	56	60.21	7	16	96	105.95	9	31	20	27
Th	6	12	17.19	30	9	23	28.86	20	4	10	14
U	2	2	1.95	−3	3	2	2.03	2	3	5	11
Pb	17	21	23.55	11	23	17	17.77	4	11	22	22
La	9	30			15	51			23	14	15
Ce	21	63			37	98			49	33	34
Nd	5	25			13	40			23	9	13

Table 2 (*continued*)

Analysis No.	12970	12971			12972	12973			12974	12975	12976
Sample No.	X-1	X-2			X-3	X-4			X-5	X-6	X-7
Rare earth elements (in ppm, ID)			(ICP-MS)	Diff (%)			(ICP-MS)	Diff (%)			
La	9.290	31.84	30.88	−3	17.63	62.79	63.64	1			
Ce	18.99	63.78	61.67	−3	36.63	118.0	119.62	1			
Nd	7.002	22.09	22.47	2	13.27	41.91	45.05	7			
Sm	1.334	3.592	3.62	1	2.454	6.441	7.01	8			
Eu	0.193	0.469	0.59	20	0.221	0.575	0.72	20			
Gd	1.116	2.765	2.70	−2	1.900	4.664	4.62	−1			
Tb			0.39				0.72				
Dy	1.227	2.146	2.18	2	1.763	3.692	3.92	6			
Ho			0.42				0.72				
Er	0.831	1.235	1.10	−13	1.046	1.933	1.94	0			
Tm			0.20				0.30				
Yb	0.970	1.305	1.33	2	1.173	1.874	2.13	12			
Lu	0.148	0.202	0.22	9	0.187	0.317	0.33	4			
Eu/Eu*	0.47	0.44			0.30	0.31					

Analysis No.	12977	12978	12979	12980	12981	12982	12983	12984	12985
Sample No.	L-1	L-2	L-3	L-4	L-5	L-6	L-7	L-8	L-9
Major elements (wt.%, by XRF)									
SiO_2	73.49	73.52	73.97	76.87	78.18	77.29	77.19	77.53	76.84
Al_2O_3	13.73	13.79	13.44	11.95	12.02	11.78	11.93	11.54	12.30
FeO*	0.65	1.31	1.00	0.83	0.79	0.93	0.87	0.75	0.63
MnO	0.02	0.02	0.02	0.08	0.07	0.07	0.09	0.05	0.04
MgO	0.31	0.30	0.23	0.06	0.06	0.07	0.10	0.01	0.04
CaO	0.65	0.56	0.71	0.40	0.42	0.29	0.40	0.21	0.24
Na_2O	3.97	4.00	3.90	3.89	3.93	3.92	4.00	3.77	4.09
K_2O	4.89	4.38	4.35	3.99	3.94	3.81	3.88	4.03	4.30
TiO_2	0.25	0.28	0.27	0.13	0.13	0.14	0.12	0.11	0.09
P_2O_5	0.07	0.07	0.08	0.02	0.02	0.04	0.02	0.02	0.02
LOI	0.89	0.77	0.71	0.39	0.30	0.37	0.29	0.42	0.36
Total	98.9	99.0	98.7	98.6	99.9	98.7	98.9	98.4	99.0
Al/(Ca+Na+K)	1.05	1.12	1.08	1.04	1.04	1.06	1.04	1.05	1.04
Al/(Na+K)	1.16	1.22	1.21	1.11	1.12	1.11	1.11	1.09	1.08
Q	30.63	32.62	33.68	38.77	39.48	39.96	38.67	40.57	36.59
Or	29.48	26.35	26.24	24.01	23.39	22.89	23.25	24.30	25.77
Ab	34.27	34.46	33.68	33.51	33.40	33.73	34.33	32.55	35.10
An	2.82	2.36	3.06	1.89	1.96	1.20	1.88	0.93	1.08
Mg-Hy	0.79	0.76	0.58	0.15	0.15	0.18	0.25	0.03	0.10
Fe-Hy									
Ap	0.17	0.17	0.19	0.05	0.05	0.09	0.05	0.05	0.05
Ilm	0.04	0.04	0.04	0.17	0.15	0.15	0.20	0.11	0.09
Ru	0.23	0.26	0.25	0.04	0.05	0.06	0.02	0.05	0.05
Cor	0.91	1.65	1.24	0.56	0.58	0.79	0.48	0.66	0.54
Hem	1.81	1.84	1.83	1.71	1.71	1.72	1.70	1.69	1.68
Mag									
DI	97.20	95.79	96.66	98.18	98.23	97.78	98.13	98.35	98.54

(continued on next page)

Table 2 (*continued*)

Analysis No.	12977	12978	12979	12980	12981	12982	12983	12984			12985		
Sample No.	L-1	L-2	L-3	L-4	L-5	L-6	L-7	L-8			L-9		
Trace elements (in ppm, by XRF)									(ICP-MS)	Diff (%)		(ICP-MS)	Diff (%)
Nb	14.9	13.3	14.0	15.1	14.9	14.2	16.2	14.6	12.36	−18	18.1	16.05	−13
Zr	153	159	153	114	95	115	109	90	82.95	−8	77	72.85	−6
Y	10	7	10	7	4	7	7	2	6.92	71	4	10.60	62
Sr	142	145	164	26	27	28	24	17	18.15	6	6	6.04	1
Rb	220	195	194	157	155	153	163	173	178.18	3	208	223.42	7
Co	<1	1	1	<1	<1	<1	<1	<1	0.55		<1	0.17	
V	12	28	22	6	7	6	5	6	2.69	−123	4	1.26	−218
Ni	1	2	2	1	1	1	1	1	2.18	54	1	2.76	64
Cr	2	4	3	2	3	3	2	5	−1.00	599	3	0.27	−1025
Ba	796	488	501	116	96	100	91	106	95.30	−11	10	14.57	31
Ga	17	17	16	16	17	16	17	16	16.78	5	18	19.13	6
Cu	2	0	<1	<1	<1	<1	<1	<1	1.07		<1	1.32	
Zn	17	24	38	26	26	33	30	46	46.26	1	25	27.67	10
Th	22	18	18	19	20	19	22	18	22.17	19	22	27.03	19
U	10	6	5	5	6	4	5	5	4.05	−23	4	3.48	−15
Pb	12	13	12	24	26	24	26	27	27.62	2	32	33.25	4
La	35	28	27	25	21	25	24	18			17		
Ce	68	59	57	49	42	47	47	38			34		
Nd	22	19	20	12	9	14	9	10			6		
Rare earth elements (in ppm, ID)									(ICP-MS)	Diff (%)		(ICP-MS)	Diff (%)
La	41.38			25.78				16.74	17.24	3	16.87	19.84	15
Ce	71.31			48.16				34.90	36.80	5	31.26	31.41	0
Nd	23.47			13.21				7.268	8.27	12	6.921	7.37	6
Sm	3.839			1.882				0.992	1.00	0	0.889	0.98	9
Eu	0.620			0.201				0.103	0.11	3	0.067	0.07	8
Gd	3.090			1.320				0.740	0.59	−26	0.717	0.76	6
Tb									0.15			0.14	
Dy	2.535			1.474				0.828	0.91	9	0.956	1.00	4
Ho									0.21			0.27	
Er	1.463			1.161				0.718	0.73	1	0.953	0.84	−14
Tm									0.12			0.17	
Yb	1.525			1.644				1.176	1.22	4	1.694	1.66	−2
Lu	0.238			0.283				0.204	0.18	−11	0.308	0.29	−7
Eu/Eu*	0.54			0.37				0.36			0.25		

Analysis No.	12986	12987	12988	12989	12990	12991	12992	12993	12974
Sample No.	YE-1	YE-2	YE-3	YE-4	YE-5	YE-6	YE-7	YE-8	YE-9
Major elements (wt.%, by XRF)									
SiO_2	77.02	75.97	73.93	76.10	71.33	77.19	76.51	75.88	73.59
Al_2O_3	11.49	12.35	13.42	12.60	14.62	12.18	12.09	12.40	13.51
FeO*	1.29	0.91	1.11	0.99	1.46	0.94	0.93	0.86	1.30
MnO	0.04	0.02	0.03	0.01	0.05	0.02	0.02	0.02	0.04
MgO	0.04	0.10	0.31	0.21	0.28	0.09	0.00	0.05	0.22
CaO	0.11	0.27	0.41	0.25	0.88	0.26	0.28	0.25	0.54
Na_2O	3.59	3.74	4.12	3.65	4.57	4.00	3.94	3.73	3.64
K_2O	4.44	4.65	4.91	4.76	4.82	4.31	4.44	4.72	5.15
TiO_2	0.15	0.14	0.22	0.15	0.26	0.08	0.08	0.16	0.20

Table 2 (*continued*)

Analysis No.	12986	12987	12988	12989	12990	12991			12992			12993	12974
Sample No.	YE-1	YE-2	YE-3	YE-4	YE-5	YE-6			YE-7			YE-8	YE-9
Major elements (wt.%, by XRF)													
P_2O_5	0.01	0.02	0.05	0.03	0.08	0.03			0.03			0.02	0.06
LOI	0.56	0.54	0.47	0.51	0.38	0.27			0.23			0.43	0.39
Total	98.7	98.7	99.0	99.3	98.7	99.4			98.6			98.5	98.6
Al/(Ca + Na + K)	1.05	1.06	1.04	1.08	1.02	1.04			1.02			1.06	1.08
Al/(Na + K)	1.07	1.10	1.11	1.13	1.15	1.08			1.07			1.10	1.17
Q	39.60	36.42	30.43	36.34	24.63	37.16			36.70			36.26	31.95
Or	26.72	27.99	29.45	28.48	28.96	25.70			26.69			28.43	30.97
Ab	30.94	32.24	35.39	31.28	39.32	34.15			33.91			32.18	31.35
An	0.49	1.23	1.73	1.06	3.91	1.10			1.21			1.13	2.33
Mg-Hy	0.10	0.25	0.78	0.53	0.71	0.23						0.13	0.56
Fe-Hy													
Ap	0.02	0.05	0.12	0.07	0.19	0.07			0.07			0.05	0.14
Ilm	0.09	0.04	0.07	0.02	0.11	0.04			0.04			0.04	0.09
Ru	0.11	0.12	0.19	0.14	0.21	0.06			0.06			0.14	0.16
Cor	0.61	0.73	0.71	1.07	0.48	0.54			0.37			0.76	1.13
Hem	1.73	1.72	1.79	1.73	1.82	1.67			1.67			1.74	1.77
Mag													
DI	97.75	97.88	97.00	97.16	96.82	98.11			98.51			98.00	96.60
Trace elements (in ppm, by XRF)							(ICP-MS)	Error (%)		(ICP-MS)	Error (%)		
Nb	22.8	18.1	16.0	16.2	15.7	21.6	23.56	8	22.8	24.09	5	16.7	12.8
Zr	220	126	180	143	209	149	154.94	4	146	152.05	4	136	115
Y	6	5	8	10	16	<1	3.96		<1	4.27		7	6
Sr	10	23	72	35	161	23	23.18	1	21	19.88	−6	27	141
Rb	226	193	180	192	160	160	169.10	5	161	175.12	8	191	274
Co	<1	<1	<1	<1	<1	<1	0.29		<1	0.24		<1	<1
V	5	6	11	7	15	7	4.70	−49	5	4.96	−1	5	14
Ni	2	1	1	2	1	<1	0.44		1	1.49	33	1	2
Cr	4	3	2	3	3	4	1.18	−240	6	1.05	−469	3	2
Ba	42	184	511	258	634	104	95.79	−9	100	87.87	−14	222	450
Ga	21	18	17	17	19	23	26.06	12	24	25.93	7	17	18
Cu	<1	<1	<1	<1	<1	<1	1.14		<1	1.17		<1	2
Zn	81	29	31	24	38	14	13.70	−2	13	11.11	−17	28	22
Th	15	27	17	26	16	74	80.23	8	74	80.94	9	21	27
U	4	7	4	5	5	9	6.71	−34	11	7.80	−41	8	7
Pb	49	21	18	15	20	15	15.79	5	16	17.33	8	22	17
La	29	29	32	32	29	13			10			29	24
Ce	61	57	64	62	61	23			19			59	50
Nd	18	13	23	20	20	4			3			16	17
Rare earth elements (in ppm, ID)							(ICP-MS)	Error (%)		(ICP-MS)	Error (%)		
La	35.41				29.33	22.53	21.48	−5	13.77	12.81	−7		23.68
Ce	63.94				63.23	21.84	21.26	−3	16.42	15.95	−3		43.40
Nd	19.56				23.21	2.250	2.30	2	1.998	2.53	21		14.63
Sm	3.259				4.054	0.240	0.24	−1	0.246	0.28	12		2.545
Eu	0.283				0.77	0.070	0.06	−15	0.068	0.10	30		0.472
Gd	2.286				3.274	0.230	0.20	−18	0.228	0.25	7		1.918
Tb							0.04			0.04			

(continued on next page)

Table 2 (*continued*)

Analysis No.	12986	12987	12988	12989	12990	12991			12992			12993	12974
Sample No.	YE-1	YE-2	YE-3	YE-4	YE-5	YE-6			YE-7			YE-8	YE-9
Rare earth elements (in ppm, ID)							(ICP-MS)	Error (%)		(ICP-MS)	Error (%)		
Dy	1.942				2.884	0.260	0.29	11	0.296	0.29	−1		1.612
Ho							0.08			0.09			
Er	1.181				1.716	0.360	0.32	−13	0.407	0.32	−27		1.010
Tm							0.08			0.11			
Yb	1.471				1.816	1.000	0.95	−5	1.102	1.08	−2		1.288
Lu	0.236					0.230	0.21	−9	0.253	0.24	−3		0.228
Eu/Eu*	0.30				0.63	0.880			0.87				0.63

Total iron as FeO*.
Al/(Ca + Na + K) and Al/(Na + K) are molar ratios.
DI = Differentiation Index.

MAT-262 mass spectrometer. $^{87}Sr/^{86}Sr$ ratios were normalized against the value of $^{86}Sr/^{88}Sr = 0.1194$. Seven replicate analyses on NBS-987 Sr standard yielded $^{87}Sr/^{86}Sr = 0.710259 \pm 6$.

Rb–Sr isochron ages were calculated using the regression program of ISOPLOT (Ludwig, 1999). Input errors are 2% for $^{87}Rb/^{86}Sr$ and 0.005% for $^{87}Sr/^{86}Sr$. Unless specified, the errors quoted in age computation represent ± 2 standard deviations (2σ).

4.4. Ar–Ar analyses

Four K-feldspar separates were prepared for $^{40}Ar/^{39}Ar$ analyses. Pure mineral separates were obtained by magnetic separation followed by heavy liquid treatment and final handpicking under the microscope to remove all visible impurities. Aliquots of feldspar separates were wrapped in aluminum foil packets and stacked in an aluminum canister with irradiation standard LP-6 biotite which has a K–Ar age of 127.7 ± 1.4 Ma (Odin et al., 1982). The samples were irradiated in the VT-C position of the THOR Reactor at Tsing-Hua University (Taiwan) for 8 h, receiving a neutron flux of 1.566×10^{13} n/cm/s. The mean J values were 0.0010427 and 0.0010265 for two irradiation procedures in June and December, 1996. The variation in flux across the samples is less than 0.8%. After irradiation, samples were removed from the Al foil packets, and loaded into fused quartz boats which were previously degassed in vacuo at 1200 °C for 3 h. During the $^{40}Ar/^{39}Ar$ experiments, all samples were heated stepwise with a Lindberg resistance furnace following a 30 min/step schedule from 500 to 1200 °C. The released gas was purified with a Ti sponge and Zr–Al getters and measured with a Varian-MAT GD150 mass spectrometer run in a static mode at the National Taiwan University. All Ar isotope analyses were corrected for system blanks, neutron-induced interferences, radioactive decay and mass discrimination. The quoted uncertainties (at 1σ) include systematic errors in J value and age of the flux monitors, but exclude the errors in the interference corrections. A more detailed description of the analytical procedures and data reduction was given by Lo and Lee (1994). The results of $^{40}Ar/^{39}Ar$ analyses are shown as age spectrum and isotope correlation plots. Plateau ages were calculated from the sum total of the gas compositions for the successive temperature steps with ages agreeing within 2σ. Data regression for the isotope correlation diagrams was done using the cubic least-squares fitting scheme of York (1969).

5. Major and trace element abundances

The results of chemical analyses for the three plutons are listed in Table 2. The granites are silica-rich, with SiO_2 ranging from 69% (X-4) to 78% (L-5). They have high contents of alkalis, with $K_2O = 3.8–5.2\%$ and $Na_2O = 3.1–4.6\%$ (except for enclave X-5), but low abundances in Fe_2O_3 (total Fe) (0.6–4.4%), MnO (0.0–0.3%), MgO (0.0–1.2%), CaO (0.1–1.1%), TiO_2 (0.1–0.6%) and P_2O_5 (0.0–0.2%). Al_2O_3 ranges from 11.5% to 14.6%. The

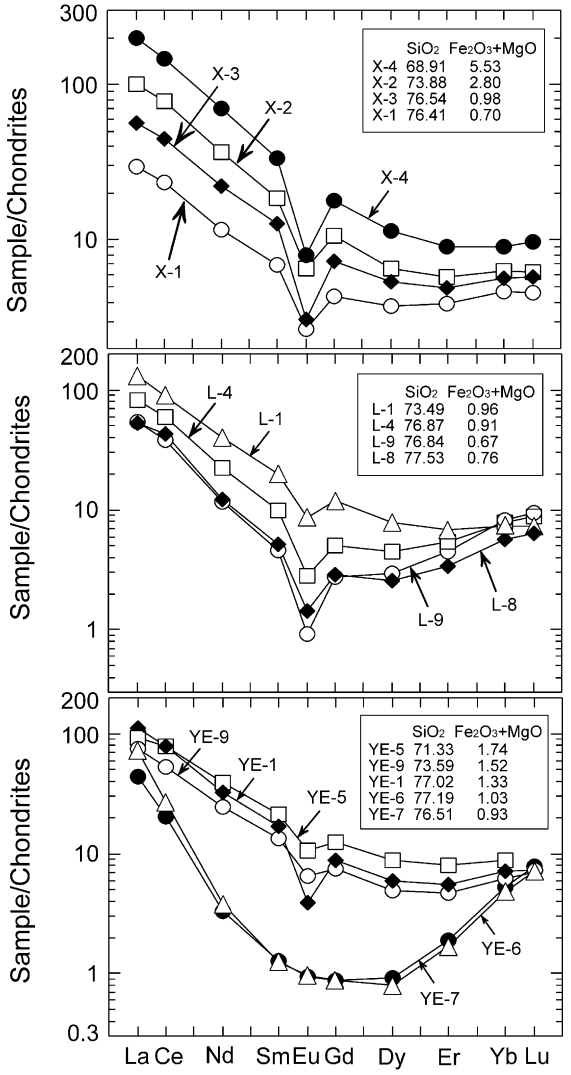

Fig. 3. Chondrite-normalized REE patterns for the granites from NE China. Note that the REE abundances are inversely proportional to SiO_2 contents. The distinctive concave patterns of YE-6 and YE-7 may be related to the fractionation of apatite and allanite.

Shand's index A/CNK ($Al_2O_3/[CaO+K_2O+Na_2O]$, in mole) indicates that these rocks are peraluminous and expressed by the presence of normative corundum (Table 2). All the samples are silica-oversaturated with 27–41% of normative quartz (except enclave X-5).

Chondrite-normalized REE patterns (Fig. 3) invariably show light REE enrichment and significant negative Eu anomalies. In each pluton, total REE abundances decrease with increasing SiO_2 (DI, Fig. 3). However, samples YE-6 and YE-7 are distinctive for their low and concave REE patterns with no Eu anomalies. The generation of this pattern is not precisely understood, but it could be modeled by fractionation of apatite, allanite, titanite or monazite (see later discussion). In the primitive mantle normalized variation diagrams (Fig. 4), all the granitic rocks show characteristic negative anomalies in Ba, Nb, Sr, P, Eu and Ti, and a positive anomaly for Pb.

6. Geochronology

The results of zircon SHRIMP analyses are listed in Table 3, Rb–Sr isotopic data for whole-rock (WR) and mineral samples are given in Table 4 and Ar isotopic analyses are presented in Table 5. The age results for the three plutons are discussed below.

6.1. Xinhuatun pluton

SHRIMP U–Pb analyses on 10 zircon grains from sample X-4 are shown in Fig. 5a. Eight grains give a tight range of $^{206}Pb/^{238}U$ ratios, yielding an age of 184 ± 4 Ma. These define a single population of weak to moderately zoned crystals with well-developed crystal faces, typical of magmatic zircons. The slightly older and younger grains have a similar morphology and are not readily distinguishable from the main population. The older grain is most likely inherited from a slightly older source, whereas the younger grain is reversely discordant and the Pb isotopic system shows post-crystallization disturbance (Table 3). We therefore take the age of 184 ± 4 Ma to represent the time of granitic intrusion. Whole-rock Rb–Sr data of this pluton define an isochron of 173 ± 3 Ma with $(^{87}Sr/^{86}Sr)_i$ (initial Sr isotopic ratio) = 0.7045 ± 1 (Fig. 6a). If the enclave data (X-5) are excluded, the calculated age remains the same. The Rb–Sr age is slightly younger than the zircon age. We also analyzed biotites and feldspars from samples X-2 and X-4 in order to constrain the minimum age of intrusion and estimate the rate of magma cooling. The results yielded two

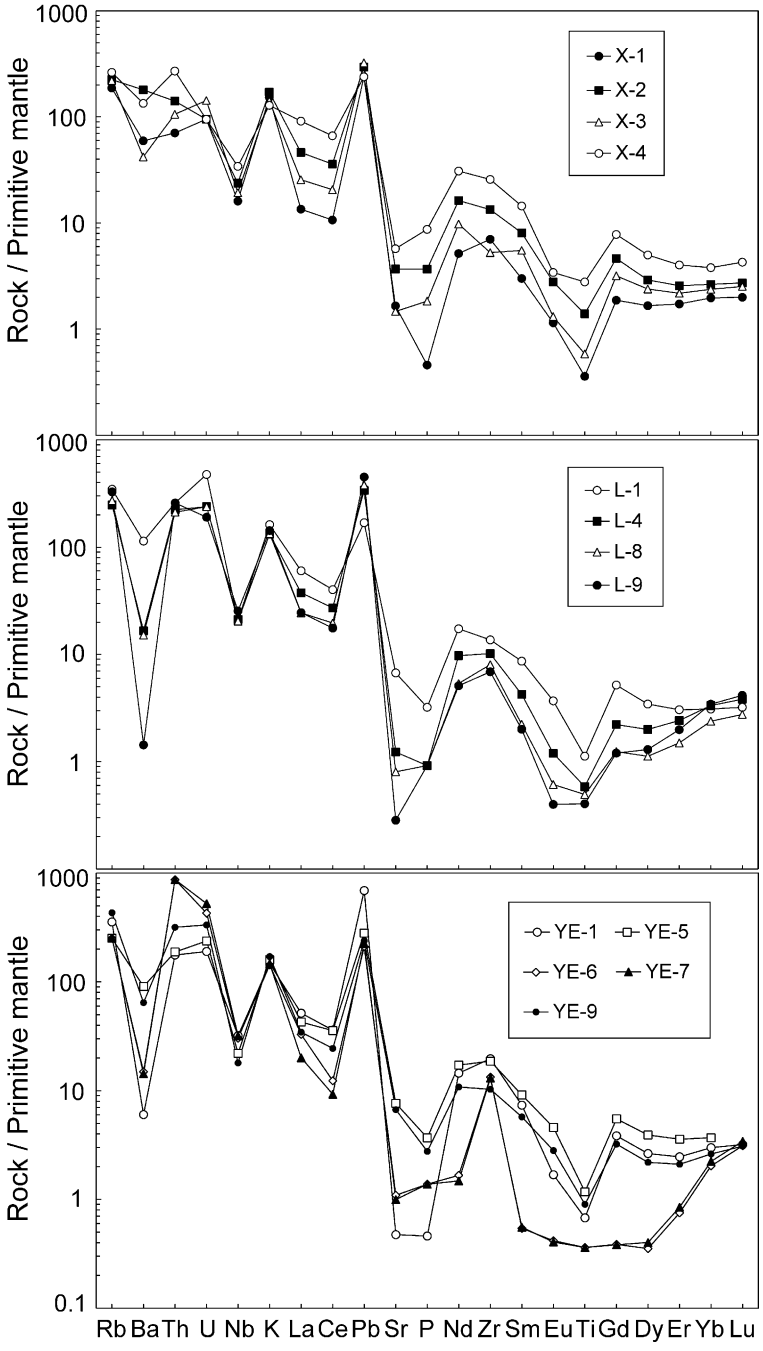

Fig. 4. Primitive-mantle (PM) normalized spidergrams for the granites from NE China. Elements are arranged in the order of decreasing incompatibility from left to right. The primitive mantle values (in ppm) are from Sun and McDonough (1989).

biotite ages (Bi-WR and Bi-Kf) of 165 ± 4 and 167 ± 4 Ma for X-2 (Fig. 6b) and 160 ± 3 and 162 ± 4 Ma for X-4 (Fig. 6c). These biotite ages correspond to the time when biotite was cooled to its blocking temperature of about 300–250 °C (Jager et al., 1967). The low initial $^{87}Sr/^{86}Sr$ ratios of 0.7045 indicate that the protoliths of the granites were dominated by depleted mantle-derived materials, such as basaltic rocks or granitoids with short crustal residence time. Assuming the magmatic temperature was 750 °C (Chappell et al., 2000), the rate of cooling calculated from the zircon U–Pb, WR Rb–Sr isochron and biotite ages yields ≈ 25 °C/Ma.

6.2. Lamashan pluton

Nine WR Rb–Sr isotopic analyses yielded an excellent isochron age of 154 ± 3 Ma with $(^{87}Sr/^{86}Sr)_i$ = 0.7049 ± 2 (Fig. 7), which is interpreted as the emplacement age of the Lamashan pluton. Zircon separation was attempted, but no satisfactory SHRIMP analysis was obtained on the few available grains. Because the Lamashan granites are poor in biotite, this phase could not be separated for isotopic analysis. On the other hand, two K-feldspar separates, from samples L-1 and L-4, were analyzed for Ar isotopes. As shown in Fig. 8, except for some discordance in the low-temperature steps of L-1 K-feldspar,

Table 3
SHRIMP U–Pb–Th analytical data of zircons for the granites in NE China

Spot	U (ppm)	Th (ppm)	Th/U	Pb (ppm)	Isotopic ratios							Age (Ma)					
					$^{204}Pb/^{206}Pb$	$^{207}Pb^a/^{206}Pb^a$	1σ	$^{206}Pb^a/^{238}U$	1σ	$^{207}Pb^a/^{235}U$	1σ	$^{206}Pb^a/^{238}U$	1σ	$^{207}Pb^a/^{235}U$	1σ	$^{207}Pb^a/^{206}Pb^a$	1σ
Xinhuatun pluton (X-4)																	
x4-1	574	481	0.84	18	0	0.04968	124	0.0281	7	0.193	7	179	4	179	6	180	58
x4-2	760	393	0.52	23	0	0.05134	100	0.0293	7	0.207	7	186	4	191	6	256	45
x4-3	408	102	0.25	12	0.00034	0.05348	178	0.0299	7	0.221	9	190	4	202	8	349	75
x4-4	862	840	0.97	36	0.00299	0.05373	306	0.0298	7	0.221	14	189	4	203	12	360	129
x4-5	185	69	0.37	5	0.00017	0.04801	288	0.0289	7	0.191	13	184	5	178	11	100	135
x4-6	318	112	0.35	9	0	0.05098	212	0.0292	7	0.205	10	185	4	189	9	240	96
x4-7	511	345	0.67	18	0.00016	0.04966	189	0.0328	8	0.225	10	208	5	206	9	179	88
x4-8	522	479	0.92	16	0.00020	0.04731	136	0.0266	6	0.173	7	169	4	162	6	68	64
x4-9	465	340	0.73	15	0.00009	0.05027	158	0.0288	7	0.200	8	183	4	185	7	208	73
x4-10	588	160	0.27	16	0.00017	0.05036	154	0.0279	6	0.193	8	177	4	180	7	212	71
Yiershi pluton (YE-1)																	
YE1-2	1154	1386	1.20	26	0.00023	0.04775	214	0.0190	4	0.125	7	121	3	120	6	88	101
YE1-3	525	377	0.72	12	0	0.05110	233	0.0216	4	0.152	8	138	3	144	7	245	105
YE1-4	534	461	0.86	13	0.00012	0.05222	192	0.0220	5	0.159	7	140	3	149	6	295	84
YE1-4a	436	389	0.89	12	0.00023	0.03795	388	0.0226	5	0.118	13	144	3	113	11	0	121
YE1-5	476	351	0.74	11	0.00065	0.05185	238	0.0216	4	0.154	8	138	3	146	7	279	105
YE1-6	773	700	0.91	19	0	0.04884	206	0.0215	4	0.145	7	137	3	137	6	140	95
YE1-7	4125	5493	1.33	114	0.00002	0.04821	410	0.0220	4	0.146	3	140	2	139	3	110	20
YE1-9	428	433	1.01	9	0.00012	0.05119	330	0.0176	5	0.124	9	112	3	119	8	249	148
YE1-10	533	391	0.73	13	0.00003	0.05032	116	0.0214	4	0.149	5	137	3	141	4	210	53
YE1-11	441	426	0.96	11	0	0.04966	129	0.0213	4	0.146	5	136	3	139	4	179	61
YE1-12	4918	6032	1.23	117	0.00002	0.04891	92	0.0195	4	0.132	4	125	2	126	3	144	44
YE1-13	4852	5779	1.19	113	0.00011	0.04860	93	0.0193	4	0.129	4	123	2	123	3	129	44
YE1-14	4625	5675	1.23	120	0.00002	0.04868	43	0.0210	4	0.141	3	134	2	134	3	133	20
YE1-15	4287	5382	1.26	112	0.00001	0.04826	41	0.0211	4	0.140	3	134	2	133	3	112	19
YE1-16	399	367	0.92	10	0.00003	0.04912	292	0.0210	4	0.142	9	134	3	135	8	154	131
YE1-17	453	331	0.73	10	0.00019	0.04693	124	0.0211	4	0.136	5	134	3	130	4	51	57

[a] ^{208}Pb corrected.

Table 4
Rb–Sr-isotopic compositions of granites in NE China

Analysis No.	Sample No.	Rb (ppm)	Sr (ppm)	$^{87}Rb/^{86}Sr$	$^{87}Sr/^{86}Sr$	$2\sigma_m$	$(^{87}Sr/^{86}Sr)_i$
Xinhuatun							
12970	X-1	119	35	9.86	0.728612	6	0.7055
12971	X-2	143	98	5.31	0.717756	6	0.7053
	Bi	409.6	14.96	80.66	0.894020	6	
	Kf	203.6	106.1	5.56	0.715879	6	
12972	X-3	140	31	13.10	0.736430	6	0.7057
12973	X-4	167	121	4.00	0.714201	7	0.7048
	Bi	592.8	18.93	92.44	0.915324	8	
	Kf	237.3	120.1	5.72	0.715362	8	
	Pl	19.1	281.4	0.20	0.704936	6	
12974	X-5	125	413	0.88	0.706616	5	0.7046
12975	X-6	142	33	12.48	0.734809	6	0.7055
12976	X-7	154	28	15.97	0.744306	7	0.7068
Lamashan							
12977	L-1	206.5	135.9	4.40	0.714372	8	0.7047
12978	L-2	186.0	144.3	3.73	0.713009	7	0.7048
12979	L-3	186.5	154.5	3.49	0.712291	5	0.7047
12980	L-4	151.3	25.95	16.92	0.741003	9	0.7040
12981	L-5	146.7	27.41	15.53	0.739380	7	0.7054
12982	L-6	145.5	27.86	15.10	0.737437	5	0.7044
12983	L-7	156.3	23.97	18.93	0.745549	7	0.7041
12984	L-8	165.8	18.05	26.72	0.761829	5	0.7033
12985	L-9	198.4	6.42	91.07	0.898993	7	0.6996
Yiershi							
12986	YE-1	211.2	9.83	62.91	0.833145	7	0.7026
12987	YE-2	182.8	22.51	23.60	0.754149	7	0.7052
12988	YE-3	169.2	71.15	6.89	0.719483	7	0.7052
	Bi	799.5	7.46	328.8	1.325615	8	
12989	YE-4	181.8	34.32	15.37	0.734849	7	0.7030
12990	YE-5	149.0	159.4	2.70	0.710403	6	0.7048
	Bi	861.0	7.05	378.2	1.479904	9	
12991	YE-6	153.2	22.81	19.50	0.743859	7	0.7034
12992	YE-7	152.4	21.41	20.67	0.747255	7	0.7044
12993	YE-8	179.0	25.63	20.28	0.746042	7	0.7040
12974	YE-9	258.0	137.7	5.43	0.715591	7	0.7043

$(^{87}Sr/^{86}Sr)_i$ values are calculated using the whole-rock Rb–Sr isochron ages.

both K-feldspar separates display flat age spectra with well-defined plateaus for >75% of the $^{39}Ar_K$ released. The gas compositions for the plateau steps provide plateau ages of 128.0 ± 0.6 (1σ) Ma for L-1 and 120.9 ± 0.5 Ma for L-4 (Fig. 8a and b). These plateau ages are consistent with the intercept ages obtained from the regression of data for the plateau steps in the isotope correlation diagrams (126.6 ± 2.8 Ma for L-1 K-feldspar and 121.5 ± 1.3 Ma for L-4 K-feldspar) (Fig. 8c and d). Nevertheless, these $^{40}Ar/^{39}Ar$ plateau ages (128–121 Ma) are significantly younger (by about 30 Ma) than the WR Rb–Sr isochron age of 154 Ma. Considering the K-feldspar Ar blocking temperature of ca. 150 °C (McDougall and Harrison, 1988), the age data suggest that the average cooling rate was ca. 20 °C/Ma.

6.3. Yiershi pluton

The results of 16 SHRIMP analyses on 12 zircon grains from sample YE-1 are shown in Fig. 5b. The main population of 12 analyses gave a tightly con-

Table 5
Results of $^{40}Ar/^{39}Ar$ incremental heating experiments for A-type granites from ECAOB

T (°C)	Cum. $^{39}Ar_K$	Atmos. (%)	$^{36}Ar/^{39}Ar$	$^{37}Ar/^{39}Ar$	$^{38}Ar/^{39}Ar$	$^{40}Ar/^{39}Ar$	$^{40}Ar/^{36}Ar$	Date (Ma)
YE-1 (K-feldspar)								
550	0.097	42.431	0.16843E+00	0.41815E−05	0.60615E−01	0.11733E+03	0.69660E+03	122.2 ± 0.9
600	0.132	8.953	0.22388E−01	0.11459E−04	0.16454E−01	0.73920E+02	0.33017E+04	121.7 ± 2.5
650	0.167	8.423	0.21185E−01	0.39426E−03	0.21976E−01	0.74354E+02	0.35098E+04	123.1 ± 1.6
700	0.198	10.937	0.27960E−01	0.12862E−04	0.23211E−01	0.75572E+02	0.27029E+04	121.7 ± 1.3
800	0.265	30.873	0.10073E+00	0.16996E−02	0.45477E−01	0.96438E+02	0.95742E+03	120.6 ± 1.1
870	0.325	18.177	0.50615E−01	0.11357E−02	0.31036E−01	0.82314E+02	0.16263E+04	121.8 ± 3.9
920	0.432	26.557	0.83566E−01	0.37997E−05	0.39642E−01	0.93012E+02	0.11130E+04	123.5 ± 0.8
1120	0.577	22.681	0.67276E−01	0.29570E−03	0.40495E−01	0.87679E+02	0.13033E+04	122.6 ± 0.8
1070	0.703	19.504	0.55915E−01	0.19395E−02	0.41796E−01	0.84745E+02	0.15156E+04	123.3 ± 0.9
1100	0.813	14.328	0.39039E−01	0.36732E−05	0.38863E−01	0.80543E+02	0.20631E+04	124.7 ± 0.8
1150	0.959	11.189	0.29318E−01	0.15145E−03	0.32720E−01	0.77455E+02	0.26419E+04	124.3 ± 0.8
1200	1.000	19.538	0.54916E−01	0.35175E−02	0.32838E−01	0.83086E+02	0.15130E+04	120.9 ± 1.7
Sample mass = 103.4 mg								
J value = 0.00103754 ± 0.00000615								
Integrated date = 122.9 ± 0.8 Ma								
Plateau date = 123.5 ± 0.5 Ma (550–1150 °C)								
YE-4 (K-feldspar)								
550	0.190	26.344	0.9174E−01	0.1584E−01	0.3595E−01	0.1029E+03	0.1122E+04	137.2 ± 0.8
600	0.317	3.467	0.9071E−02	0.1764E−01	0.1497E−01	0.7731E+02	0.8522E+04	135.1 ± 1.2
650	0.418	0.004	0.1008E−04	0.2529E−02	0.1814E−01	0.7525E+02	0.7467E+07	136.2 ± 0.9
700	0.504	0.120	0.3070E−03	0.1546E−01	0.1321E−01	0.7492E+02	0.2440E+06	135.5 ± 0.8
750	0.560	3.154	0.7823E−02	0.5170E−01	0.2227E−01	0.7321E+02	0.9357E+04	128.6 ± 1.9
800	0.601	0.008	0.2493E−04	0.1748E−01	0.2329E−01	0.7270E+02	0.2916E+07	131.8 ± 2.4
850	0.646	0.007	0.2272E−04	0.1577E−01	0.2004E−01	0.7436E+02	0.3273E+07	134.7 ± 2.5
900	0.683	3.574	0.8728E−02	0.1429E−01	0.1957E+01	0.7215E+02	0.8267E+04	126.3 ± 3.5
950	0.753	10.320	0.2786E−01	0.2069E−01	0.2752E−01	0.7980E+02	0.2864E+04	129.8 ± 1.9
1000	0.791	3.840	0.9781E−02	0.7130E−02	0.2701E−01	0.7528E+02	0.7697E+04	131.2 ± 4.6
1057	0.847	3.948	0.1012E−01	0.1446E−01	0.3673E−01	0.7574E+02	0.7485E+04	131.9 ± 3.3
1100	0.916	7.161	0.1931E−01	0.1516E−01	0.3556E−01	0.7968E+02	0.4127E+04	134.0 ± 1.9
1150	0.991	21.478	0.6575E−01	0.1887E−01	0.4370E−01	0.9048E+02	0.1376E+04	128.9 ± 1.2
1212	1.000	29.035	0.8567E−01	0.1174E−03	0.1174E+00	0.8722E+02	0.1018E+04	112.8 ± 11.6
Sample mass = 38.0 mg								
J value = 0.0010427 ± 0.0000412								
Integrated date = 133.4 ± 0.7 Ma								
Plateau date = 133.6 ± 0.7 Ma (550–1150 °C)								
L-1 (K-feldspar)								
550	0.069	46.211	0.27035E+00	0.97914E−05	0.91580E−01	0.17291E+03	0.63956E+03	167.3 ± 1.8
600	0.102	20.655	0.65419E−01	0.20976E−04	0.32957E−01	0.93619E+02	0.14311E+04	134.8 ± 2.6
650	0.127	29.260	0.99307E−01	0.26442E−04	0.44735E−01	0.10032E+03	0.10102E+04	129.0 ± 3.3
700	0.155	29.253	0.96011E−01	0.24074E−04	0.40002E−01	0.97015E+02	0.10105E+04	124.9 ± 2.9
750	0.179	29.641	0.88354E−01	0.71556E−02	0.31387E−01	0.88110E+02	0.99724E+03	113.2 ± 3.5
800	0.203	30.875	0.10037E+00	0.28653E−04	0.27446E−01	0.96092E+02	0.95738E+03	121.0 ± 2.8
850	0.231	32.140	0.10307E+00	0.54013E−02	0.39086E−01	0.94793E+02	0.91967E+03	117.3 ± 1.7
900	0.266	18.877	0.53484E−01	0.31758E−02	0.27349E−01	0.83750E+02	0.15659E+04	123.7 ± 2.6
950	0.310	12.901	0.34234E−01	0.15420E−04	0.29150E−01	0.78441E+02	0.22913E+04	124.4 ± 1.4
1000	0.376	12.860	0.34697E−01	0.21055E−02	0.27692E−01	0.79754E+02	0.22986E+04	126.4 ± 2.0
1050	0.467	11.619	0.31679E−01	0.32355E−03	0.26027E−01	0.80593E+02	0.25441E+04	129.5 ± 1.0
1100	0.573	18.218	0.53101E−01	0.27817E−02	0.30949E−01	0.86159E+02	0.16225E+04	128.1 ± 0.9

(continued on next page)

Table 5 (*continued*)

T (°C)	Cum. $^{39}Ar_K$	Atmos. (%)	$^{36}Ar/^{39}Ar$	$^{37}Ar/^{39}Ar$	$^{38}Ar/^{39}Ar$	$^{40}Ar/^{39}Ar$	$^{40}Ar/^{36}Ar$	Date (Ma)
L-1 (K-feldspar)								
1150	0.885	24.346	0.77465E − 01	0.10814E − 02	0.35434E − 01	0.94051E + 02	0.12141E + 04	129.3 ± 0.8
1200	1.000	27.179	0.88696E − 01	0.14392E − 02	0.37492E − 01	0.96463E + 02	0.10876E + 04	127.8 ± 1.0
Sample mass = 100.2 mg								
J value = 0.00104493 ± 0.00000615								
Integrated date = 130.2 ± 0.8 Ma								
Plateau date = 128.0 ± 0.6 Ma (900 – 1150 °C)								
L-4 (K-feldspar)								
550	0.222	18.711	0.5156E − 01	0.4303E − 02	0.2263E − 01	0.8145E + 02	0.1580E + 04	120.4 ± 0.5
600	0.312	3.050	0.7042E − 02	0.1011E − 01	0.1539E − 01	0.6824E + 02	0.9690E + 04	120.3 ± 0.6
650	0.377	1.844	0.4220E − 02	0.8546E − 02	0.1590E − 01	0.6762E + 02	0.1602E + 05	120.7 ± 0.8
700	0.418	3.449	0.7884E − 02	0.1246E − 01	0.1532E − 01	0.6755E + 02	0.8568E + 04	118.7 ± 0.8
750	0.449	2.045	0.4631E − 02	0.1654E − 01	0.1721E − 01	0.6689E + 02	0.1444E + 05	119.2 ± 1.1
800	0.470	7.703	0.1767E − 01	0.3680E − 01	0.3715E − 01	0.6779E + 02	0.3836E + 04	114.0 ± 2.0
850	0.495	6.527	0.1536E − 01	0.4395E − 01	0.1625E − 01	0.6952E + 02	0.4526E + 04	118.2 ± 1.8
900	0.523	8.002	0.1943E − 01	0.1324E − 03	0.2077E − 01	0.7179E + 02	0.3695E + 04	120.1 ± 1.2
950	0.563	9.298	0.2283E − 01	0.9601E − 02	0.2002E − 01	0.7258E + 02	0.3179E + 04	119.7 ± 1.0
1000	0.604	10.456	0.2539E − 01	0.3106E − 01	0.1980E − 01	0.7175E + 02	0.2826E + 04	116.9 ± 1.5
1050	0.646	6.519	0.1549E − 01	0.1383E − 01	0.1785E − 01	0.7022E + 02	0.4534E + 04	119.4 ± 1.0
1100	0.695	4.758	0.1121E − 01	0.1627E − 01	0.1811E − 01	0.6966E + 02	0.6211E + 04	120.6 ± 1.5
1150	0.885	6.780	0.1681E − 01	0.1013E − 01	0.1753E − 01	0.7329E + 02	0.4360E + 04	124.1 ± 0.6
1200	1.000	11.146	0.2865E − 01	0.4716E − 02	0.2038E − 01	0.7599E + 02	0.2652E + 04	122.7 ± 0.5
Sample mass = 103.4 mg								
J value = 0.0010427 ± 0.00000412								
Integrated date = 120.9 ± 0.5 Ma								
Plateau date = 120.9 ± 0.5 Ma (550 – 1200 °C)								

J value: Weighted mean of one fusion of irradiation standard LP-6 Biotite, having a K–Ar age of 127.7 ± 1.4 Ma (Odin et al., 1982).
T (°C) = Temperature with uncertainty of ± 2 °C.
The date is obtained by using the following equations:

$$\text{Date} = \frac{1}{\lambda}\ln\left(1 + J\frac{^{40}Ar^*}{^{39}Ar_K}\right), \text{ and } \frac{^{40}Ar^*}{^{39}Ar_K} = \frac{\left[^{40}Ar/^{39}Ar\right]_m - 295.5\left[^{36}Ar/^{39}Ar\right]_m + 295.5\left[^{36}Ar/^{37}Ar\right]_{Ca}\left[^{37}Ar/^{39}Ar\right]_m}{1 - \left[^{39}Ar/^{37}Ar\right]_{Ca}\left[^{37}Ar/^{39}Ar\right]_m} - \left[\frac{^{40}Ar}{^{39}Ar}\right]_K$$

where [ ]$_{Ca}$ and [ ]$_K$ = isotope ratios of argon extracted from irradiated calcium and potassium salts (values cited in the text) and [ ]$_m$ = isotope ratio of argon extracted from irradiated unknown.

Date (Ma) = the date calculated using the following decay constants: $\lambda_\epsilon = 0.581 \times 10^{-10}$ year^{-1}; $\lambda_\beta = 4.962 \times 10^{-10}$ year^{-1}; $\lambda = 5.543 \times 10^{-10}$ year^{-1}; $^{40}K/K = 0.01167$ at.% (Steiger and Jäger, 1977).
Uncertainty for $^{40}Ar^*$ and $^{39}Ar_K$ volumes are ± 5%.
Cum. ^{39}Ar = cumulative fractions of $^{39}Ar_K$ and $^{40}Ar^*$ released in each step.
The quoted error is one standard deviation and does not include the error in the standard error, or the error in the interference corrections.
Integrated Date = the date and error calculated from the sum total gas from all steps; the error includes the error in J value.
Plateau Date = the data and error calculated from the sum total gas from those steps, the ages of which fall within 2 S.D. of each other; the error includes the error in J value.

strained $^{206}Pb/^{238}U$ age of 137 ± 2 Ma. The zircons are stubby with some oscillatory zoning, indicative of a magmatic origin. The slightly younger population at 123 ± 6 Ma are morphologically similar, but generally have higher U and Th concentrations and Th/U ratios >1.0. Together with the younger grain of 112 ± 3 Ma, they probably reflect various amounts of recent Pb loss, although it should be noted that they remain

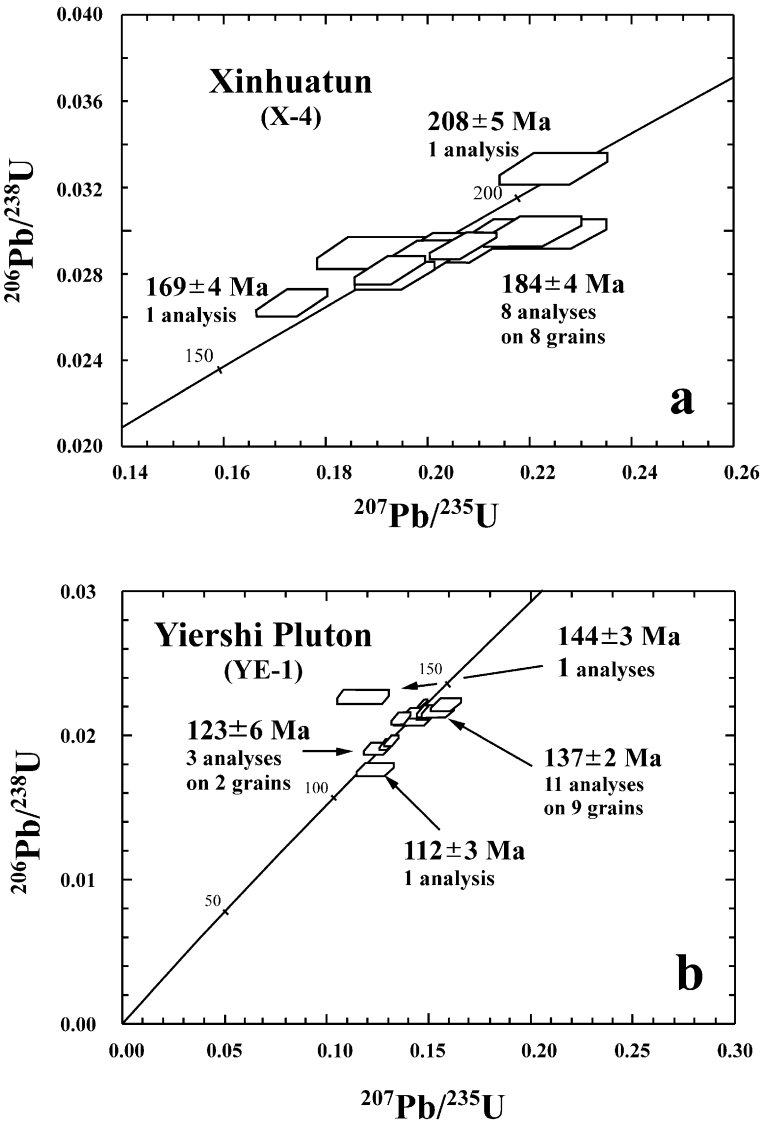

Fig. 5. U–Pb concordia diagram for the granites in NE China. (a) X-4 (Xinhuatun Pluton); (b) YE-1 (Yiershi Pluton).

reasonably concordant. We therefore interpret the weighted mean age of 137 ± 2 Ma for the main zircon population as representing the time of granitic emplacement.

Nine WR samples defined a Rb–Sr WR isochron age of 143 ± 5 Ma with $(^{87}Sr/^{86}Sr)_i = 0.7049 \pm 6$ (MSWD = 7.7; Fig. 9a). The Rb–Sr isochron age is identical with the zircon age within the error limits. Although sample YE-1 had undergone intense weathering as suggested by O isotope (see the companion paper), the weathering has apparently not disturbed the Rb–Sr isotopic system. Biotite-WR isochrons for samples YE-3 and YE-5 give ages of 133 ± 3 Ma ($(^{87}Sr/^{86}Sr)_i = 0.7065 \pm 4$, Fig. 9b) and 134 ± 3 Ma ($(^{87}Sr/^{86}Sr)_i = 0.7053 \pm 4$, Fig. 9c), respectively. Ar–Ar analyses of K-feldspar separates

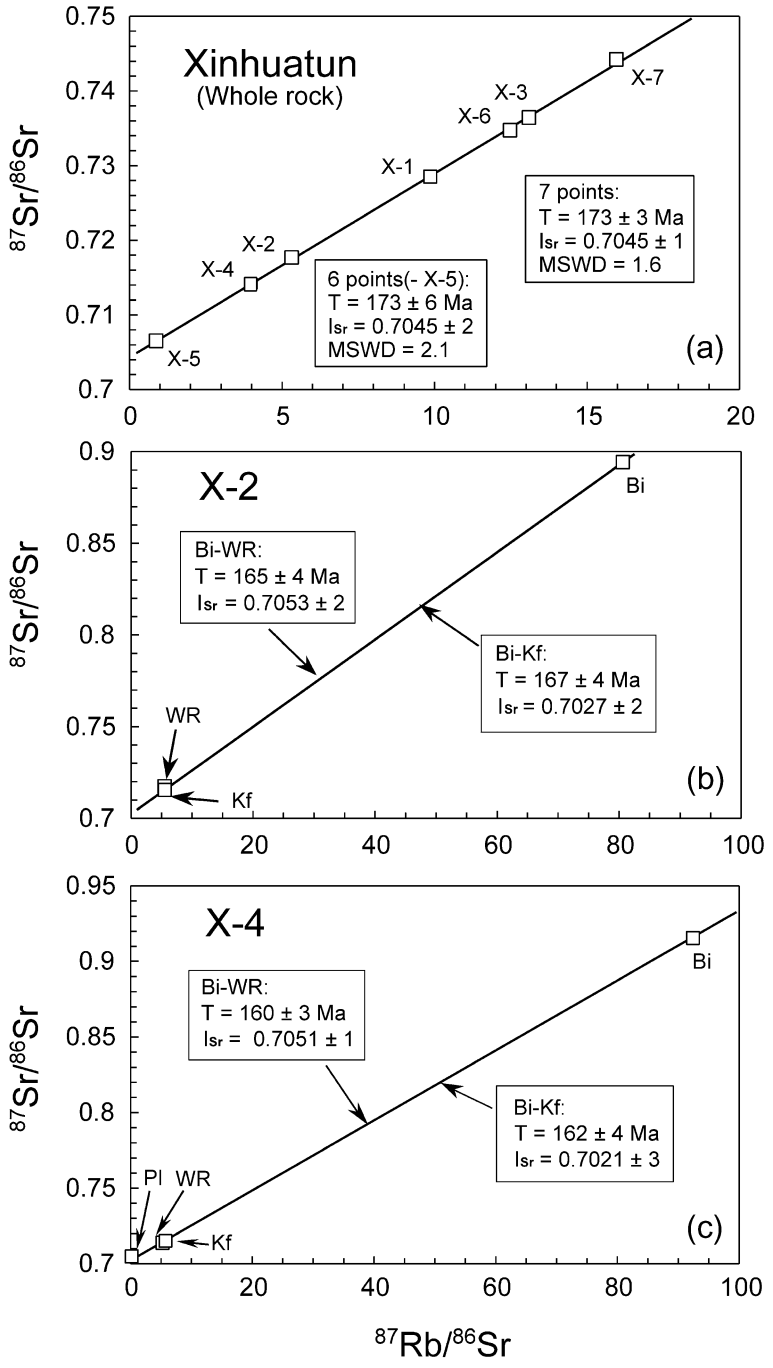

Fig. 6. Rb–Sr isochron diagrams of the Xinhuatun Pluton. (a) Whole-rock (WR) isochron; (b) and (c): internal isochrons for samples X-2 and X-4, respectively.

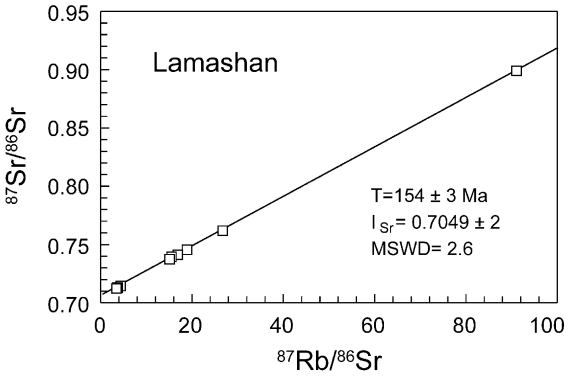

Fig. 7. Rb–Sr WR isochron diagram of the Lamashan Pluton.

from two granite samples (YE-1 and YE-4) yield plateau ages of 123.5 ± 0.5 and 133.6 ± 0.7 Ma, respectively (Fig. 10a and b). In the isotope correlation diagrams, regression of data for plateau steps gives intercept ages of 125.8 ± 0.8 and 133.6 ± 0.7 Ma, which are in complete agreement with their respective plateau ages (Fig. 10c and d). The Ar ages of YE-4 are identical to the biotite Rb–Sr ages, but the Ar age of sample YE-1 is the same as the second group of zircon ages in the same sample, which indicates that each individual sample has a different cooling history. If the younger age of 126 Ma is taken, then a cooling rate of 45 °C/Ma (early) to 20 °C/Ma (late) is obtained.

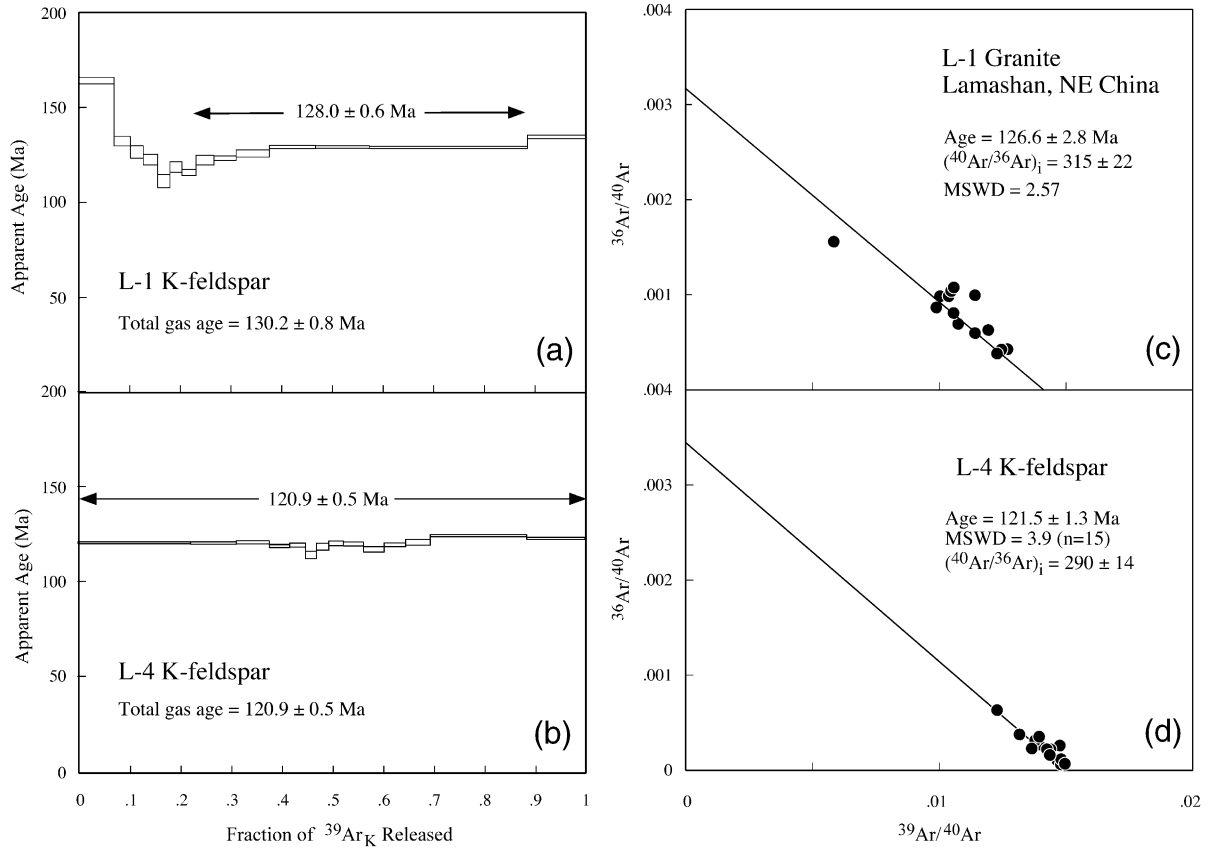

Fig. 8. $^{40}Ar/^{39}Ar$ age spectra and $^{36}Ar/^{40}Ar$–$^{39}Ar/^{40}Ar$ isotope correlation diagrams for K-feldspars extracted from two samples of the Lamashan Pluton. In the age spectra (a and b), boxes represent the relative fraction of $^{39}Ar_K$ released in heating steps and extend vertically to ± 1σ. In the isotope correlation diagrams (c and d), solid circles indicate the gas compositions for plateau steps, which were incorporated into the data regression. Error ellipses represent ± 1σ.

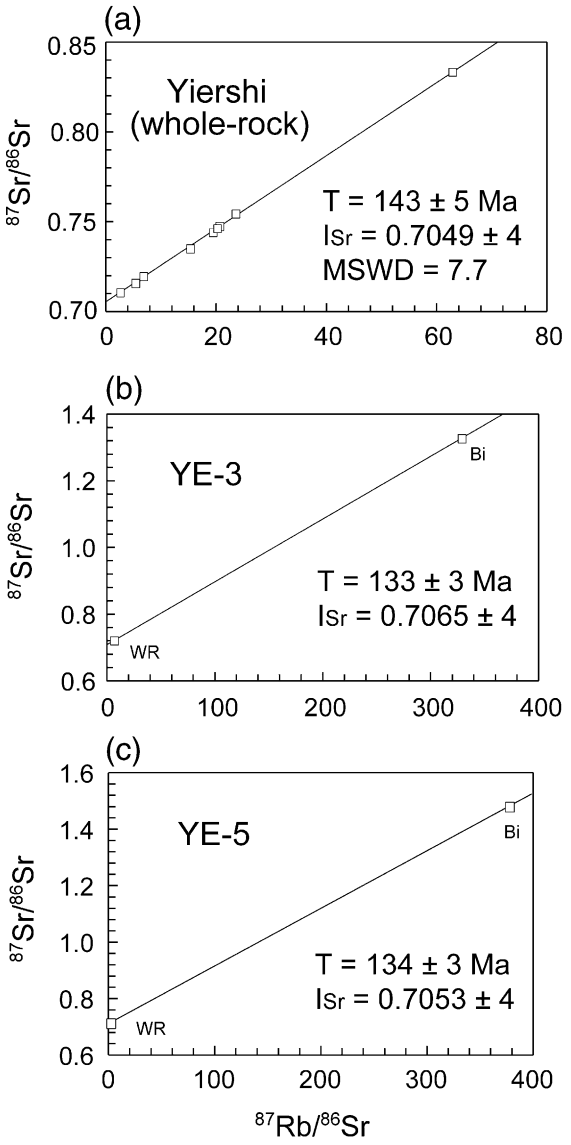

Fig. 9. Rb–Sr WR isochron diagram of the Yiershi Pluton. (a) WR Rb–Sr isochron; (b) and (c): biotite-WR isochrons for samples YE-3 and YE-5, respectively.

The above age pattern, namely, zircon U–Pb age ≈ WR Rb–Sr isochron age>biotite-WR Rb–Sr isochron age>feldspar $^{40}Ar/^{39}Ar$ age, has been found to be systematic in granitic plutons since mineral ages often record the cooling history of the rocks, whereas zircon U–Pb and whole-rock Rb–Sr isochron ages are taken to reflect the emplacement age. In addition, the flat age spectra and the consistency between the plateau and intercept ages suggest that since the closure of the Ar isotope clock, the samples have not been significantly disturbed by later-stage events. They have only experienced a simple cooling history since their emplacement (Harrison, 1990).

The cooling histories of the three plutons are summarized in Fig. 11. Assuming magmatic intrusion temperatures of 800–700 °C (Chappell et al., 2000), the earlier-formed Xinhuatun and Lamashan plutons seem to have slower cooling rates than the later Yiershi pluton, at least in the initial stage when biotite was cooled to its blocking temperature of ca. 300–250 °C (Jager et al., 1967). This was followed by a lower cooling rate of ca. 20 °C/Ma. The Lamashan pluton has no biotite age as a constraint, but it probably had the slowest cooling rate and longest cooling time (Δt = ca. 30 Ma) from emplacement to the closure of K-feldspar K–Ar isotope systems (~ 150–200 °C; McDougall and Harrison, 1988).

Combining our present and recent age data with previous work in this region (Fang, 1992; HBGMR, 1993; Wu et al., 2002), it can be concluded that Phanerozoic granitic emplacement in NE China took place from the late Paleozoic to late Mesozoic, with culmination in the period of 210–140 Ma. This is about 120 to 140 Ma younger than the widespread post-orogenic A-type granites (300–280 Ma) in Northern Xinjiang, central Inner Mongolia and the Great Xing'an Ranges (Hong et al., 1994; Wang et al., 1994; Han et al., 1997; Sun et al., 2001).

Precise age determination is of utmost importance for any tectonic evolution models. Sengör et al. (1993) and Sengör and Natal'in (1996a,b) published a series of papers on the evolution of the Central Asian Orogenic Belt and used the "magmatic front" as a new type of structural marker in their reconstruction of tectonic evolution. However, available precise age data were scarce, and the validity of the "magmatic front" concept based on old age information was severely hampered. In NE China, most granites were assigned late Paleozoic ages (Li and Zhao, 1984), but more recently, they have been reassigned as Indosinian (ca. 200 Ma) on the basis of a few imprecise whole-rock Rb–Sr isochron dates (HBGMR, 1993). The new age data presented here and those published in Wu et al. (2002) clearly show

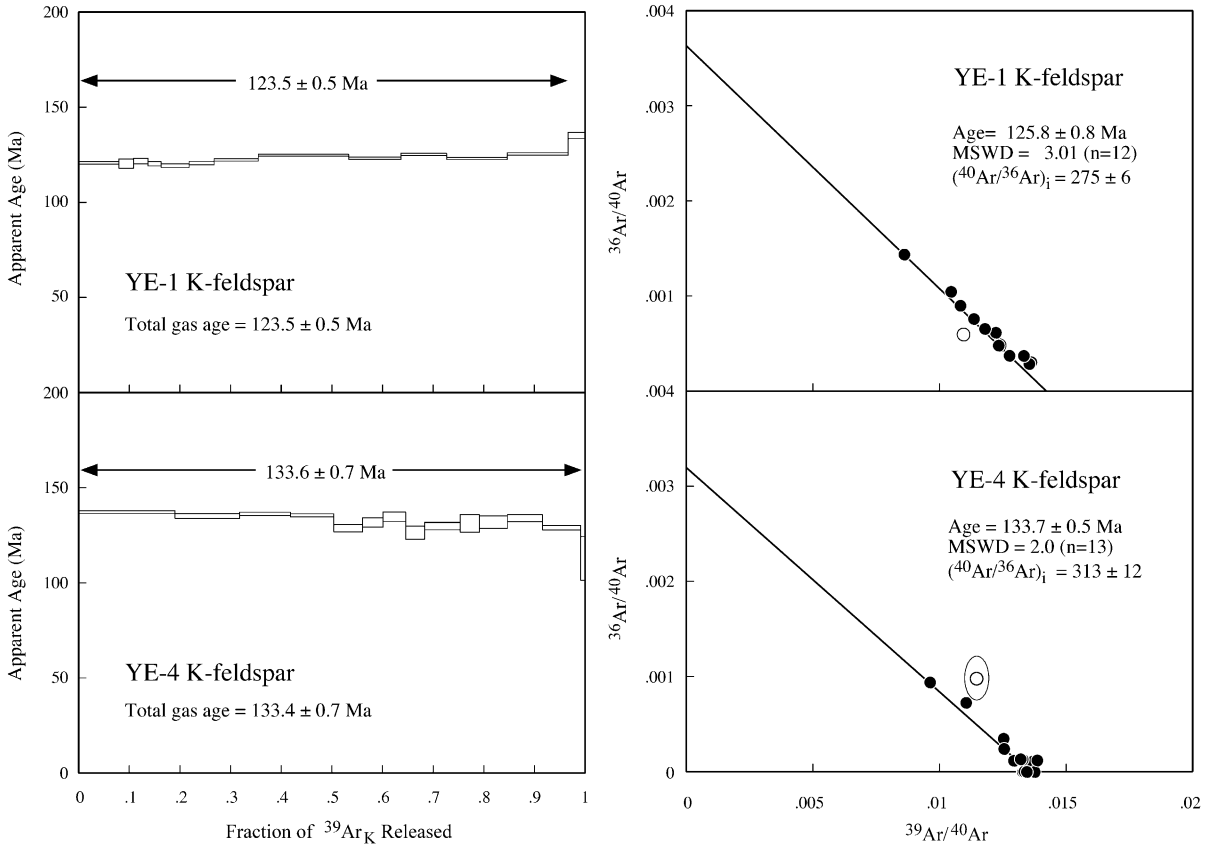

Fig. 10. $^{40}Ar/^{39}Ar$ age spectra and $^{36}Ar/^{40}Ar$–$^{39}Ar/^{40}Ar$ isotope correlation diagrams for K-feldspars extracted from samples of the Yiershi Pluton. All notations are the same as in Fig. 8.

that many of the earlier dates were erroneously assigned. Therefore, until further precise age data are obtained, any tectonic model based on the magmatic front model must involve a large uncertainty.

7. Petrogenesis

7.1. Genetic type: I-type or A-type?

Since the introduction of the terms "I-" and "S-type" granite by Chappell and White (1974), granitic rocks have commonly been divided into I-, S-, M- and A-types according to their protolith nature (Pitcher, 1982, 1993). However, distinction between different types is not always easy. This is particularly true for the case of A-type and highly differentiated I-type granites (White and Chappell, 1983; Chappell and Stephens, 1988; Chappell and White, 1992, 2001; Champion and Chappell, 1992; Landenberger and Collins, 1996; King et al., 1997, 2001). Several attempts have been made to discriminate A-types from the others (I-, S- and M-type) (e.g., Loiselle and Wones, 1979; Collins et al., 1982; Whalen et al., 1987, 1996; Sylvester, 1989; Eby, 1990, 1992). In general, A-type granites are emplaced later than I-types and they are comparatively enriched in HFSEs (high field strength element), such as Zr, Nb, Y, REE and Ga, although significant compositional overlap is also observed; for example, an early recognition of the importance of Ga enrichment

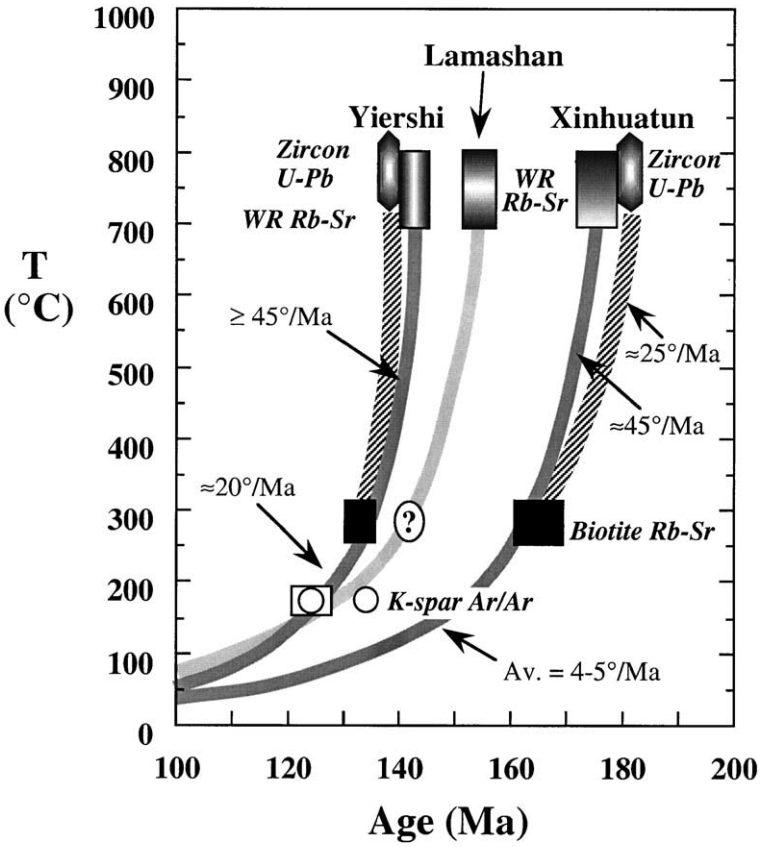

Fig. 11. Cooling paths of the three plutons.

(relative to Al) has persisted in most subsequent studies.

The granites in this study are peraluminous; most of them have A/CNK < 1.1, normative corundum < 1% and A/NK>1.0. It is also shown that P_2O_5 decreases with increasing SiO_2, whereas Pb moves in the opposite direction (Fig. 12). This feature is considered as an important criterion for distinction of I- from S-type granitoids by Chappell and White (1992). Combined with the Sr isotopic data, it is clear that the granites under study are not S-type but they belong to I- or A-types.

The granites in NE China have some similarities to A-type in their field and petrographic characteristics. However, they do not contain mafic alkaline minerals such as arfvedsonite, riebeckite, etc. The relatively low contents of Zr, Nb, Y, La, Ce, Zn and Ga strongly suggest that they belong to I-type. As proposed by Whalen et al. (1987), in some discrimination diagrams of K_2O+Na_2O, FeO*/MgO, Nb and Zr vs. Ga/Al (Fig. 13a–d), the granites straddle the fields of A- and M-, I-, S-types with small variation in Ga/Al ratios. Furthermore, in FeO*/MgO and (K_2O+Na_2O)/CaO vs. (Zr + Nb + Ce + Y) diagrams (Fig. 13e and f), most of these granites fall in the field of highly fractionated I-type. This is also confirmed by the criteria of Sylvester (1989) using the diagram of (Al_2O_3+CaO)/ $(FeO^*+Na_2O+K_2O)$ vs. $100(MgO+FeO^*+TiO_2)/SiO_2$ (not shown here), which is fairly effective in discriminating alkaline granites from calc-alkaline and strongly peraluminous granites. We therefore conclude that the granites described in this study are highly fractionated I-type granites.

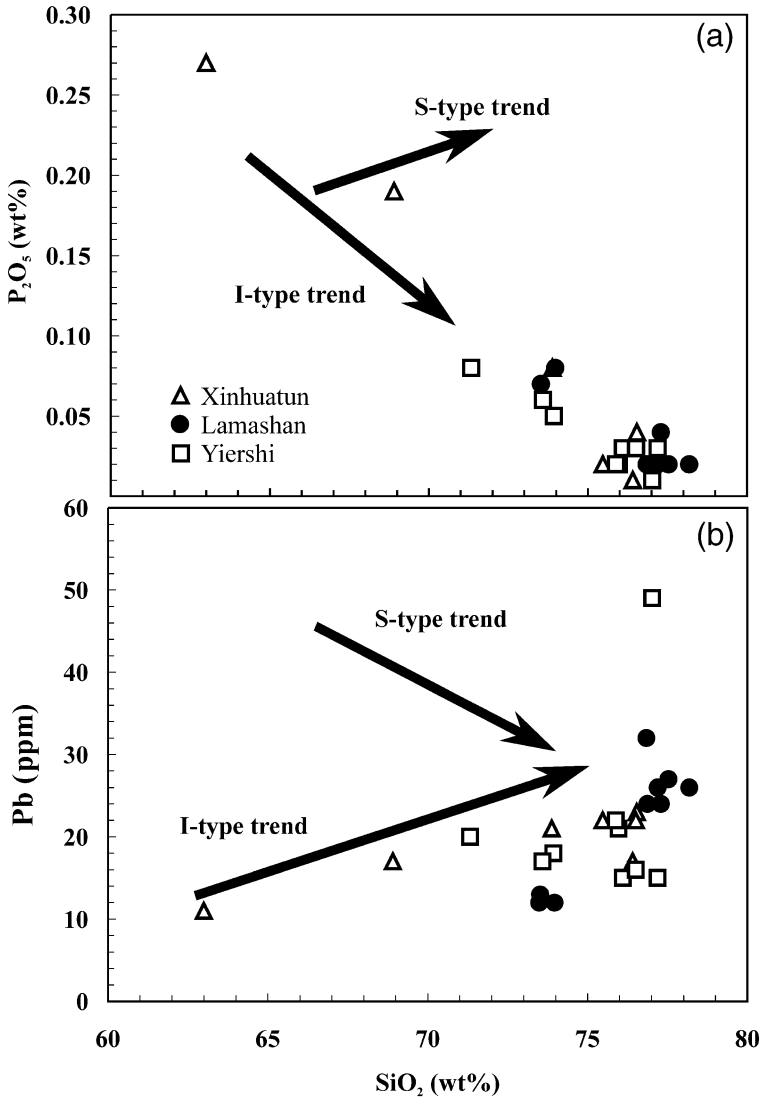

Fig. 12. (a) P_2O_5 vs. SiO_2 and (b) Pb vs. SiO_2 variation diagrams showing that the granites follow the trend of I-type proposed by Chappell and White (1992).

7.2. Fractionation processes

Advanced fractional crystallization has taken place during the formation of these granites. This is supported by the striking depletions in Ba, Sr, Nb, P, Ti and Eu shown in the spidergrams (Fig. 4). Negative Nb–Ti anomalies are considered to be related to fractionation of Ti-bearing phases (ilmenite, titanite, etc.) and negative P anomalies should result from apatite separation. Strong Eu depletion requires extensive fractionation of plagioclase and/or K-feldspar. Fractionation of plagioclase would result in negative Sr–Eu anomalies, and that of K-feldspar would produce negative Eu–Ba anomalies.

Generally, as SiO_2 increases, total REE, Sr and Ba contents decrease, whereas the Rb content is fairly

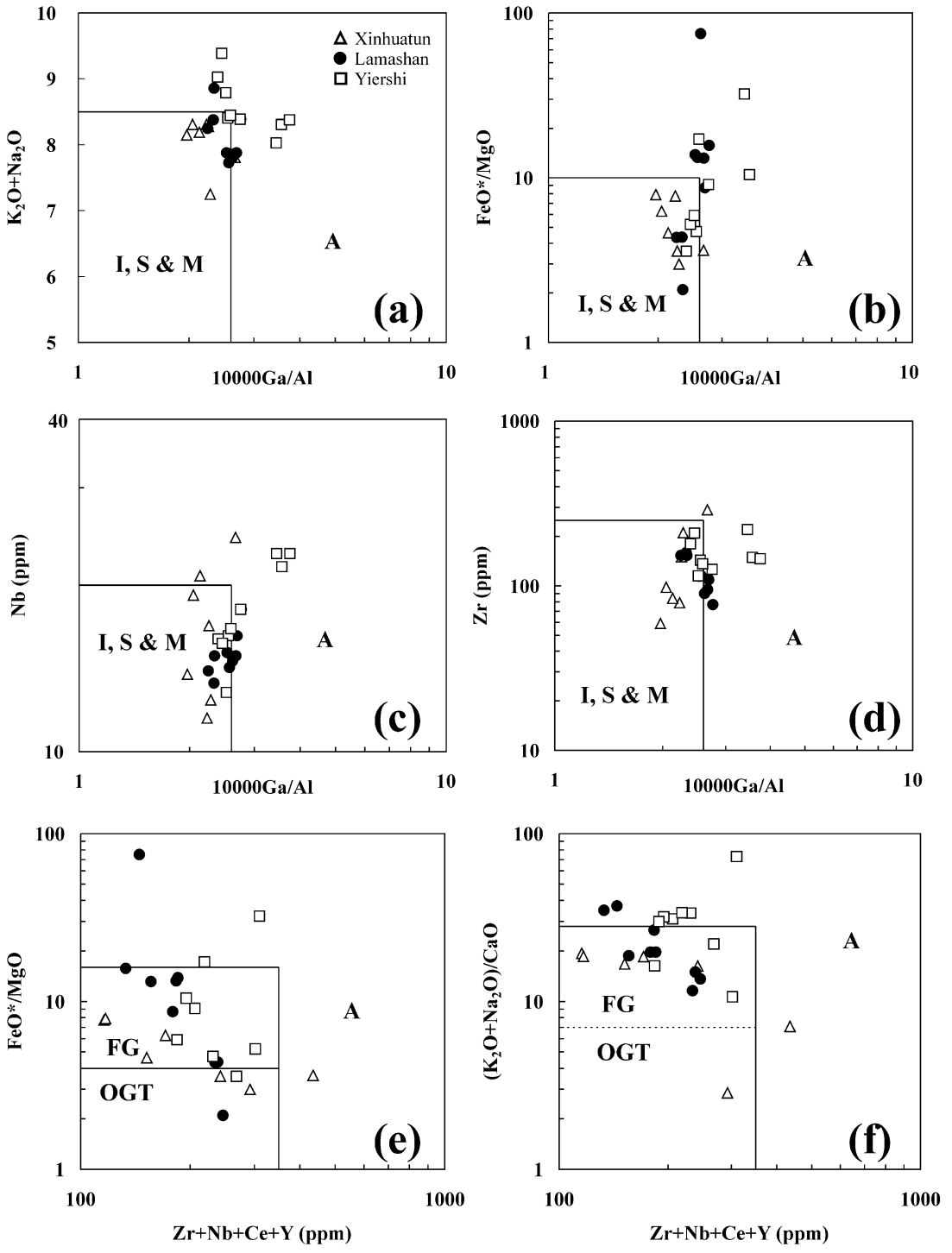

Fig. 13. (a) K_2O+Na_2O, (b) FeO*/MgO, (c) Nb, (d) Zr vs. 10000 Ga/Al and (e) FeO*/MgO, (f) $(K_2O+Na_2O)/CaO$ vs. (Zr+Nb+Ce+Y) classification diagrams (Whalen et al., 1987), indicating that the granites from NE China are transitional between the I-, S-, M- and A-types (a–d) or highly fractionated. FG: Fractionated felsic granites; OGT: unfractionated M-, I- and S-type granites.

constant at about 200 ppm. In log–log diagrams of Ba vs. Sr and Ba/Sr vs. Sr (Fig. 14), it appears that Sr concentration decreases sharply from about 500 to <10 ppm, whereas Ba changes little in the early stage of crystallization but decreases rapidly in the later stage. This is explained by fractionation of plagioclase in the early stage, and by separation of plagioclase and biotite, rather than K-feldspar, in later stages, because the proportion of K-feldspar increases during magmatic evolution as shown by the petrography (Table 1). Low MgO content in these granites suggests separation of mafic minerals, and petrographic evidence favors a probable fractionation of biotite. The overall geochemical evolution is consistent with fractional crystallization from granodiorite, monzogranite, syenogranite to alkali-feld-

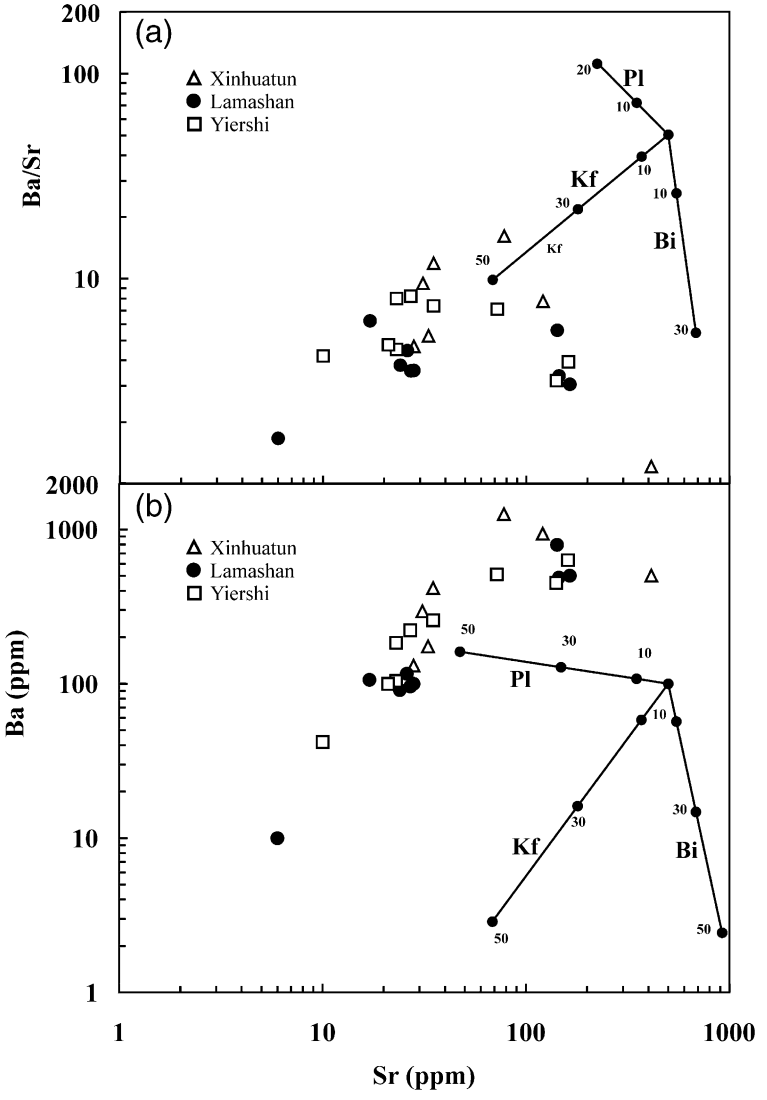

Fig. 14. (a) Ba/Sr vs. Sr and (b) Ba vs. Sr diagrams showing that fractionation of plagioclase plays an important role in the early stage of differentiation; whereas in the later stage, separation of plagioclase and biotite, rather than K-feldspar alone, appears to have controlled the variation of these elements. Partition coefficients of Sr and Ba are from Hanson (1978).

spar granite. Magma mixing or partial melting of heterogeneous sources is not required to explain the concentration patterns.

In addition to major phases, accessory minerals seem to have controlled much of the REE variation. The decrease of REE with increasing SiO_2 suggests a separation of minerals with high partition coefficients (Kd), such as apatite, titanite, zircon, allanite and monazite, which are important accessory minerals in these rocks. In a diagram of $(La/Yb)_N$ vs. La (Fig. 15), the variation of REE contents seems to be consistent with fractionation of allanite and monazite (less than 2%) and, to a lesser extent, apatite. Zircon does not seem to have exerted much influence on REE fractionation. For Xinhuatun samples, the regular decrease in REE or La content from X-4 to X-2 to X-3 to X-1 is mimicked by regular decrease in P_2O_5 and Th concentrations (Table 2), which suggests a separation of monazite instead of allanite + apatite during the differentiation process.

The distinctive REE patterns of two Yiershi samples (YE-6 and YE-7, Fig. 4) are highly unusual. Although similar patterns in granites have been reported previously (Koljonen and Rosenberg, 1974), the precise mechanism for creating these patterns is not clear. Our simple modeling suggests that a greater separation of apatite, allanite, titanite and/or monazite was probably responsible. Hornblende was not observed in any of the samples, but it could have disappeared due to fractionation. The result of modeling is presented in Table 6. As shown in Fig. 16, separation of apatite and allanite would lower overall REE abundance, enhance the concavity of REE patterns and reduce the degree of Eu anomalies from the "parental" magma with strong negative Eu anomaly, as represented by sample YE-1. Due to the similar partition coefficients, fractionation of titanite would have the same effect as apatite. Monazite is not included in the simulation test, but its effect is similar to that of allanite, only to enhance the skewness of the concavity toward HREE.

In summary, during the formation of the various granites, fractionation of feldspars, biotite, apatite, monazite and ilmenite has played an important role. Fractionation of biotite and feldspars is the main cause for the variation of major elements. At the same time, feldspars also controlled Rb, Sr and Ba abundances. The variation of REE was mainly

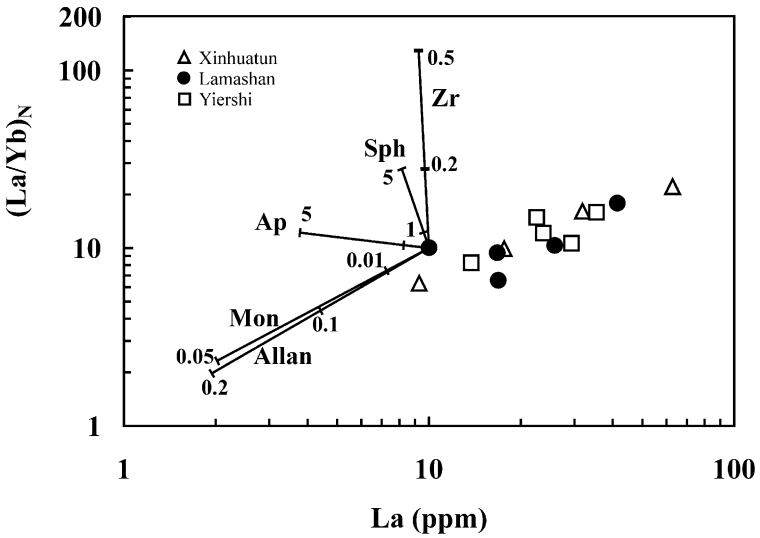

Fig. 15. $(La/Yb)_N$ vs. La diagram showing the change of REE patterns by separation of accessory minerals, especially allanite and apatite. Partition coefficients are from Arth (1976) for apatite, Green and Pearson (1986) for titanite, Mahood and Hildreth (1983) for zircon, Green et al. (1989) for allanite and Yurimoto et al. (1990) for monazite.

Table 6
Modelling of formation of concave REE patterns

	Kd (Hb)	Kd (Ap)	Kd (Aln)	Kd (Tit)	D (ApAln) (95/5)	D (HbApAln) (70/28.5/1.5)	D (ApAlnTit) (48/4/48)	Co (YE1) × chon	$C^l = Co.F^{(D-1)}$					
									$F = 0.98$ (ApAln)	$F = 0.99$ (ApAln)	$F = 0.95$ (HbApAln)	$F = 0.97$ (HbApAln)	$F = 0.98$ (ApAlnTit)	$F = 0.99$ (ApAlnTit)
La	0.75	30	1000	30	79	24	69	112.41	23.5	51.6	34.4	55.7	28.6	56.9
Ce	1.4	40	1050	42	91	28	81	78.65	12.9	32.0	19.6	34.4	15.5	35.1
Nd	4	55	900	60	97	32	91	32.87	4.7	12.5	6.7	12.8	5.3	13.3
Sm	8	60	700	75	92	33	93	16.89	2.7	6.8	3.2	6.3	2.6	6.7
Eu	5	40	50	70	41	16	55	3.92	1.8	2.6	1.8	2.5	1.3	2.3
Gd	11	60	400	75	77	31	81	8.83	1.9	4.1	1.9	3.6	1.8	4.0
Dy	12	50	200	70	58	26	66	5.98	1.9	3.4	1.7	2.8	1.6	3.1
Er	10	40	150	60	46	21	54	5.54	2.3	3.5	2.0	3.0	1.9	3.3
Yb	8	20	90	50	24	13	37	7.07	4.5	5.6	3.9	5.0	3.4	4.9
Lu	6	14	75	45	17	9	31	7.31	5.3	6.2	4.8	5.7	4.0	5.4

Partition coefficients from Arth (1976), Hanson (1978) and estimates from the literature.
Abbreviations: Hb = hornblende, Ap = apatite, Aln = allanite, Tit = titanite, chon = chondrite abundances.

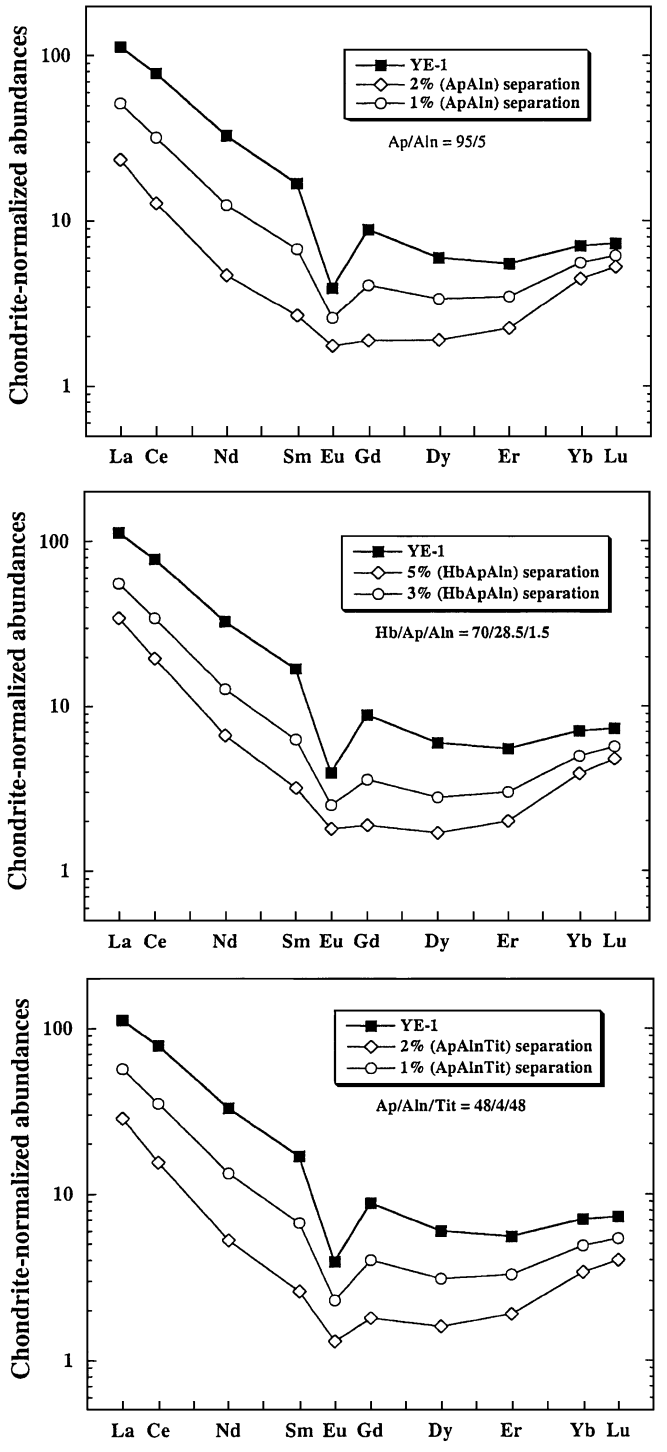

Fig. 16. REE patterns of sample YE-1 and modeled concave patterns with a variety of fractionated phase combinations. If the starting composition has a smaller negative Eu anomaly, such as that shown by YE-5 and YE-9 (Fig. 3), then this anomaly would disappear with the same degree of fractionation as indicated in the figure.

achieved by fractionation of apatite, monazite and allanite. The primary magma was probably granodioritic in view of the lithological characters of the early-crystallized products in the Xinhuatun pluton. If the nature of the enclave suite is considered, it is equally possible that the primary magma was dioritic. However, the extensive mineral fractionation makes the assessment of primary magma composition highly uncertain.

8. Conclusions

The present study leads to the following conclusions:

(1) The three studied plutons in NE China (Xinhuatun, Lamashan and Yiershi) range from granodiorite (minor), monzogranite, syenogranite to alkali-feldspar granite in lithology. The petrography is characterized by quartz and perthitic feldspar as the principal mineral phases with minor amounts of plagioclase, biotite and some accessory minerals.
(2) Zircon U–Pb SHRIMP analyses indicate that these granites were emplaced in the Jurassic (184–137 Ma), not Triassic as previously thought. Biotite-WR Rb–Sr isochrons and $^{40}Ar/^{39}Ar$ ages of feldspars suggest that they have undergone a slow cooling history, which allows extensive fractional crystallization.
(3) Geochemical study indicates that the granites are silica-rich, peraluminous and have high contents of alkalis and evident enrichment of light relative to heavy REE, with significant negative Eu anomalies. The negative anomalies of Ba, Nb, Sr, P, Eu and Ti, and positive anomaly of Pb in the spidergram, suggest that these granites have undergone advanced fractional crystallization with separation of plagioclase, biotite, K-feldspar and accessory minerals. Genetically, they are highly fractionated I-types.

Acknowledgements

Fuyuan Wu is most grateful to the laboratory staff in Rennes, particularly to Odile Henin, Joél Macé, Nicole Morin and Martine Le Coz-Bouhnik for their instructions in chemical separation, mass spectrometry and XRF analyses. R. Capdevila, Jon Patchett, M. Wilson, H.-J. Forster, Alain Cocherie and O. T. Rämö commented on earlier drafts and provided many useful suggestions. This work was supported by the National Natural Science Foundation of China (NSFC grant 4940008 to Q. Lin and 49872031 to F.Y. Wu), the State Education Commission of China (to F.Y. Wu for his stay in France) and French research programmes of "Dynamique des Transferts Terrestres" (INSU-DTT 97) and "Cycles Géochimiques" (INSU-IT 99) granted to B.M. Jahn. This is INSU Contribution No. 327. The SHRIMP facility in Perth is operated by the Western Australian Consortium, comprising Curtin University of Technology, the University of Western Australia and the Geological Survey of Western Australia. This paper is also a contribution to IGCP-420: Crustal Growth in the Phanerozoic: Evidence from Central Asia.

References

Arth, J.G., 1976. Behaviour of trace elements during magmatic processes: a summary of theoretical models and their applications. J. Res. U.S. Geol. Surv. 4, 41–47.

Champion, D.C., Chappell, B.W., 1992. Petrogenesis of felsic I-type granites: an example from northern Queensland. Trans. R. Soc. Edinb. Earth Sci. 83, 115–126.

Chappell, B.W., Stephens, W.E., 1988. Origin of infracrustal (I-type) granite magmas. Trans. R. Soc. Edinb. Earth Sci. 79, 71–86.

Chappell, B.W., White, A.J.R., 1974. Two contrasting granite types. Pac. Geol. 8, 173–174.

Chappell, B.W., White, A.J.R., 1992. I- and S-type granites in the Lachlan Fold Belt. Trans. R. Soc. Edinb. Earth Sci. 83, 1–26.

Chappell, B.W., White, A.J.R., 2001. Two contrasting granite types: 25 years later. Aust. J. Earth Sci. 48, 489–499.

Chappell, B.W., White, A.J.R., Williams, I.S., Wyborn, D., Wyborn, L.A., 2000. Lachlan fold belt granites revisited: high- and low-temperature granites and their implications. Aust. J. Earth Sci. 47, 123–138.

Collins, W.J., Beams, S.D., White, A.J.R., Chappell, B.W., 1982. Nature and origin of A-type granites with particular reference to southeastern Australia. Contrib. Mineral. Petrol. 80, 189–200.

Compston, W., Williams, I.S., Kirschvink, J.L., Zhang, Z., Ma, G., 1992. Zircon U–Pb ages for the Early Cambrian time-scale. J. Geol. Soc. (London) 149, 171–184.

Eby, G.N., 1990. The A-type granitoids: a review of their occurrence and chemical characteristics and speculations on their petrogenesis. Lithos 26, 115–134.

Eby, G.N., 1992. Chemical subdivision of the A-type granitoids: petrogenetic and tectonic implications. Geology 20, 641–644.

Fang, W.C., 1992. The Granitoids and Their Mineralizations in Jilin Province (in Chinese). Jilin Publishing House of Science and Technology, Changchun. 271 pp.

Green, T.H., Pearson, N.J., 1986. Rare-earth element partitioning between titanite and coexisting silicate liquid at high pressure and temperature. Chem. Geol. 55, 105–119.

Green, T.H., Sie, S.H., Ryan, C.G., Cousens, D.R., 1989. Proton microprobe-determined partitioning of Nb, Ta, Zr, Sr and Y between garnet, clinopyroxene and basaltic magma at high pressure and temperature. Chem. Geol. 74, 201–216.

Han, B.F., Wang, S.G., Jahn, B.M., Hong, D.W., Kagami, H., Sun, Y.L., 1997. Depleted-mantle magma source for the Ulungur River A-type granites from north Xinjiang, China: geochemistry and Nd–Sr isotopic evidence, and implication for Phanerozoic crustal growth. Chem. Geol. 138, 135–159.

Hanson, G.N., 1978. The application of trace elements to the petrogenesis of igneous rocks of granitic composition. Earth Planet. Sci. Lett. 38, 26–43.

Harrison, M.T., 1990. Some observations on the interpretation of feldspar $^{40}Ar/^{39}Ar$ results. Chem. Geol. 80, 219–229.

HBGMR (Heilongjiang Bureau of Geology and Mineral Resources), 1993. Regional Geology of Heilongjiang Province (in Chinese with English summary). Geological Publishing House, Beijing, pp. 347–438.

Hong, D.W., Huang, H.Z., Xiao, Y.J., Xu, H.M., Jin, M.Y., 1994. The Permian alkaline granites in central Inner Mongolia and their geodynamic significance. Acta Geol. Sin. 68, 219–230.

IMBGMR (Inner Mongolian Bureau of Geology and Mineral Resources), 1990. Regional Geology of Inner Mongolian Autonomous Region (in Chinese with English summary). Geological Publishing House, Beijing. 725 pp.

Jager, E., Niggli, E., Wenk, E., 1967. Rb–Sr altersbestimmungen an glimmern der zentralalpen. Beitr. Geol. Karte Shweiz N. F. 134, 1–67.

Jahn, B.M., Cornichet, J., Cong, B.L., Yui, T.F., 1996. Ultrahigh-ε_{Nd} eclogites from an ultrahigh-pressure metamorphic terrane of China. Chem. Geol. 127, 61–79.

Jahn, B.M, Wu, F.Y, Capdevila, R., Fourcade, S., Wang, Y.X., Zhao, Z.H., 2001. Highly evolved juvenile granites with tetrad REE patterns: the Woduhe and Baerzhe granites from the Great Xing'an (Khingan) Mountains in NE China. Lithos 59, 171–198.

JBGMR (Jilin Bureau of Geology and Mineral Resources), 1988. Regional Geology of Jilin Province (in Chinese with English summary). Geological Publishing House, Beijing, pp. 301–385.

King, P.L., White, A.J.R., Chappell, B.W., Allen, C.M., 1997. Characterization and origin of aluminous A-type granites from the Lachlan Fold Belt, Southeastern Australia. J. Petrol. 38, 371–391.

King, P.L., Chappell, B.W., Allen, C.M., White, A.J.R., 2001. Are A-type granites the high-temperature felsic granites? Evidence from fractionated granites of the Wangrah Suite. Aust. J. Earth Sci. 48, 501–514.

Koljonen, T., Rosenberg, R.J., 1974. Rare earth elements in granitic rocks. Lithos 7, 249–261.

Landenberger, B., Collins, W.J., 1996. Derivation of A-type granites from a dehydrated charnockitic lower crust: evidence from the Chaelundi complex, eastern Australia. J. Petrol. 37, 145–170.

Li, P.Z., Yu, J.S., 1993. Nianzishan miarolitic alkaline granite stock, Heilongjiang—its ages and geological implications (in Chinese with English abstract). Geochimica 22, 389–398.

Li, Z.T., Zhao, C.J., 1984. On the regularity of the tempo-spatial distribution of the granitic rocks in the northern part of northeast China. In: Xu, K.Q., Tu, G.C. (Eds.), Geology of Granites and their Metallogenetic Relations. Science Press, Beijing, pp. 195–209.

Lo, C.-H., Lee, C.Y., 1994. $^{40}Ar/^{39}Ar$ method of K–Ar age determination of geological samples using Tsing-Hua Open-pool (THOR) Reactor. J. Geol. Soc. China 37, 143–164.

Loiselle, M.C., Wones, D.R., 1979. Characteristics and origin of anorogenic granites. Geol. Soc. Am., Prog. Abstr. 11, 468.

Ludwig, K.R., 1999. Isoplot/Ex (v. 2.06)—A Geochronological Toolkit for Microsoft Excel. Spec. Publ., vol. 1a. Berkeley Geochronology Center. 49 pp.

Mahood, G., Hildreth, W., 1983. Large partition coefficients for trace elements in high-silica rhyolites. Geochim. Cosmochim. Acta 47, 11–30.

McDougall, I., Harrison, T.M., 1988. Geochronology and Thermochronology by the $^{40}Ar/^{39}Ar$ Method. Oxford Univ. Press, New York. 212 pp.

Nelson, D.R., 1999. Compilation of geochronology data, 1998, Geological Survey of Western Australia Record 1999/2, 218 pp.

Odin, G.S. et al., 1982. Interlaboratory standards for dating purpose. In: Odin, G.S. (Ed.), Numerical Dating in Stratigraphy. Wiley, Chichester, UK, pp. 123–149.

Pidgeon, R.T., Furfaro, D., Kennedy, A.K., Nemchin, A.A., van Bronswijk, W., Todt, W.A., 1994. Calibration of zircon standards for the Curtin SHRIMP II. Eighth International Conference on Geochronology, Cosmochronology and Isotope Geology, Berkeley, June 5–11. University of California, Berkeley, p. 251. Abstracts.

Pitcher, W.S., 1982. Granite type and tectonic environment. In: Hsu, K.J. (Ed.), Mountain Building Processes. Academic Press, London, pp. 19–40.

Pitcher, W.S., 1993. The Nature and Origin of Granite Blackie Academic and Professional, London. 321 pp.

Qin, K.Z., Tanaka, R., Li, W.S., Ishihara, S., 1998. The discovery of Indosinian granites in Manzhouli area: evidence from Rb–Sr isochrons (in Chinese with English abstract). Acta Petrol. Mineral. 17, 235–240.

Qin, K.Z., Li, H.M., Li, W.S., Ishihara, S., 1999. Intrusion and mineralization ages of the Wulugetushan porphyry Cu–Mo deposit, Inner Mongolia, northeastern China (in Chinese with English abstract). Geol. Rev. 45, 180–185.

Sengör, A.M.C., Natal'in, B.A., 1996a. Paleotectonics of Asia: fragments of a synthesis. In: Yin, A., Harrison, M. (Eds.), The Tectonic Evolution of Asia. Cambridge Univ. Press, New York, pp. 486–640.

Sengör, A.M.C., Natal'in, B.A., 1996b. Turkic-type orogeny and its role in the making of the continental crust. Annu. Rev. Earth Planet. Sci. 24, 263–337.

Sengör, A.M.C., Natal'in, B.A., Burtman, V.S., 1993. Evolution of the Altaid tectonic collage and Palaeozoic crustal growth in Eurasia. Nature 364, 299–307.

Steiger, R.H., Jäger, E., 1977. Subcommission on geochronology: convention on the use of decay constants in geo- and cosmochronology. Earth Planet. Sci. Lett. 36, 359–362.

Sun, S.S., McDonough, W.F., 1989. Chemical and isotopic systematics of oceanic basalts: implications for mantle composition and processes. In: Saunders, A.D., Norry, M.J. (Eds.), Magmatism in the Ocean Basins. Geol. Soc. Spec. Publ., vol. 42, pp. 313–345.

Sun, D.Y., Wu, F.Y., Li, H.M., Lin, Q., 2001. Emplacement age of the postorogenic A-type granites in northwestern Lesser Xing'an Ranges, and its relationship to the eastward extension of Suolunshan–Hegenshan–Zhalaite collisional suture zone. Chin. Sci. Bull. 46, 427–432.

Sylvester, P.J., 1989. Post-collisional alkaline granites. J. Geol. 97, 261–280.

Tang, K.D., 1990. Tectonic development of Palaeozoic fold belts at the north margin of the Sino-Korean craton. Tectonics 9, 249–260.

Tang, K.D., Wang, Y., He, G.Q., Shao, J.A., 1995. Continental-margin structure of northeast China and its adjacent areas (in Chinese with English abstract). Acta Geol. Sin. 69, 16–30.

Wang, Y.X., Zhao, Z.H., 1997. Geochemistry and origin of the Baerzhe REE–Nb–Be–Zr superlarge deposit (in Chinese with English abstract). Geochimica 26, 24–35.

Wang, S.G., Han, B.F., Hong, D.W., Xu, B.L., Sun, Y.Y., 1994. Geochemistry and tectonic significance of alkali granites along Ulungur River, Xinjiang (in Chinese with English abstract). Sci. Geol. Sin. 29, 373–383.

Whalen, J.B., Currie, K.L., Chappell, B.W., 1987. A-type granites: geochemical characteristics, discrimination and petrogenesis. Contrib. Mineral. Petrol. 95, 407–419.

Whalen, J.B., Jenner, G.A., Longstaffe, F.J., Robert, F., Gariepy, C., 1996. Geochemical and isotopic (O, Nd, Pb and Sr) constraints on A-type granite: petrogenesis based on the Topsails igneous suite, Newfoundland Appalachians. J. Petrol. 37, 1463–1489.

White, A.J.R., Chappell, B.W., 1983. Granitoid types and their distribution in the Lachlan Fold Belt, southeastern Australia. In: Roddick, J.A. (Ed.), Circum-Pacific Plutonic Terranes. Geol. Soc. Am., Mem., vol. 159, pp. 21–34.

Wilde, S.A., Dorsett-Bain, H.L., Liu, J.L., 1997. The identification of a Late Pan-African granulite facies event in northeastern China: SHRIMP U–Pb zircon dating of the Mashan Group at Liu Mao, Heilongjiang Province, China. Proc. 30th IGC: Precambrian Geol. Metamorphic Petrol., vol. 17. VSP International Publisher, Amsterdam, pp. 59–74.

Wilde, S., Zhang, X.Z., Wu, F.Y., 2000. Extension of a newly identified 500 Ma metamorphic terrain in North East China: further U–Pb SHRIMP dating of the Mashan Complex, Heilongjiang Province, China. Tectonophysics 328, 115–130.

Williams, I.S., 1998. U–Th–Pb geochronology by ion microprobe. In: McKibben, M.A., Shanks III., W.C., Ridley, W.I. (Eds.), Applications of microanalytical techniques to understanding mineralizing processes. Rev. Econ. Geol., vol. 7, pp. 1–35.

Wu, F.Y., Ye, M., Zhang, S.H., 1995. The geodynamic model of the Manzhouli–Suifenghe geoscience transect (in Chinese with English abstract). J. Earth Sci. 20, 535–539.

Wu, F.Y., Jahn, B.M., Wilde, S., Sun, D.Y., 2000. Phanerozoic crustal growth: U–Pb and Sr–Nd isotopic evidence from the granites in northeastern China. Tectonophysics 328, 89–113.

Wu, F.Y., Sun, D.Y., Li, H.M., Wang, X.L., 2001. The nature of basement beneath the Songliao Basin in NE China: geochemical and isotopic constraints. Phys. Chem. Earth (Part A) 26, 793–803.

Wu, F.Y., Sun, D.Y., Li, H.M., Jahn, B.M., Wilde, S.A., 2002. A-type granites in northeastern China: age and geochemical constraints on their petrogenesis. Chem. Geol. 187, 143–173.

Ye, M., Zhang, S.H., Wu, F.Y., 1994. The classification of the Paleozoic tectonic units in the area crossed by Manzhouli–Suifenghe geoscience transect (in Chinese with English abstract). J. Changchun Univ. Earth Sci. 24, 241–245.

York, D., 1969. Least-squares fitting of a straight line with correlated errors. Earth Planet. Sci. Lett. 5, 320–324.

Yu, J.J., Xu, Z.G., Xu, F.S., 1996. Tectonic setting of Ordovician volcanic rocks in northwestern Xiaoxing'anling, Heilongjiang Province (in Chinese with English abstract). Acta Geosci. Sin. 17, 54–64.

Yurimoto, H., Duke, E.F., Papike, J.J., Shearer, C.K., 1990. Are discontinuous chondrite-normalized REE patterns in pegmatitic granite systems the results of monazite fractionation? Geochim. Cosmochim. Acta 54, 2141–2145.

Zhang, X.Z., 1992. Heilongjiang melange: the evidence of Caledonian suture zone of the Jiamusi massif (in Chinese with English abstract). J. Changchun Univ. Earth Sci. 22, 94–101 (Special Issue: Doctoral thesis).

Zhao, X.X., Coe, R.S., Zhou, Y.X., Wu, H.R., Wang, J., 1990. New paleomagnetic results from northern China: collision and suturing with Siberia and Kazakhstan. Tectonophysics 181, 43–81.

Zonenshain, L.P., Kuzmin, M.I., Kononov, M.V., 1985. Absolute reconstructions of the Paleozoic oceans. Earth Planet. Sci. Lett. 74, 103–116.

Zonenshain, L.P., Kuzmin, M.I., Natapov, L.M., 1990. Geology of the USSR: A Plate Tectonic Synthesis. Geodyn. Ser., vol. 21. Am. Geophys. Union, Washington, DC. 242 pp.